Materials Research. 2021; 24(suppl. 1): e20210039
DOI: https://doi.org/10.1590/1980-5373-MR-2021-0039

Effect of Plasma Oxidation Treatment on Production of a SiOx/SiOxCyHz Bilayer to Protect Carbon Steel Against Corrosion

Rafael P. Ribeiro*[a], *Rita de Cássia C. Rangel*[a], *Felipe O. Fernandes*[a], *Nilson C. Cruz*[a], *Elidiane C. Rangel*[a]

[a] *Universidade Estadual Paulista (UNESP), Instituto de Ciência e Tecnologia de Sorocaba (ICTS), Laboratório de Plasmas Tecnológicos (LaPTec), Av. Três de Março, 18087-180, Sorocaba, SP, Brasil.*

Received: January 13, 2021; Revised: May 31, 2021; Accepted: June 16, 2021

Because of its excellent properties, carbon steel is a material widely used in several sectors. However, it is easily corroded when exposed to the environment. Seeking to remedy this problem, the possibility of coating carbon steel with SiO_x/$SiO_xC_yH_z$ films generated by deposition and oxidation in low-pressure plasmas was investigated. Specifically, the effects of excitation power of the oxidation plasma on layer thickness, chemical structure, elemental composition, and barrier properties of the obtained coatings were investigated. The coating of the steel with the $SiO_xC_yH_z$ film, generated by plasma in an atmosphere of hexamethyldisiloxane (HMDSO), increased the total resistance to the passage of electric current, measured by electrochemical impedance spectroscopy. However, under the condition of moderate power oxidation (50 W), the results point to the creation of a bilayer system with high resistance to electrochemical attack compared to the $SiO_xC_yH_z$ film, even though its thickness is less than this.

Keywords: Carbon steel, corrosion resistance, $SiO_xC_yH_z$, SiO_x, PECVD, plasma oxidation.

1. Introduction

Carbon steel has several attractive properties, such as high strength, good malleability, ductility, plasticity, easy forging, welding, and cutting, all combined with a relatively low cost[1-3]. Such characteristics make this metal proper to be applied in several sectors, such as in the cutting tool industry, in the manufacture of plates, sheets, bars, and tubes of the metallurgical industry, and civil construction[3-5]. However, despite its widespread use, carbon steel is not a perfect material, as it has low resistance to wear and corrosion. This ends up limiting its application in areas that need good tribological and anti-corrosion properties[1].

Although corrosion is a spontaneous process, it can be avoided. Amongst the existing prevention methods, the most used is the application of protective coatings that isolate the metal surface from the environment[6-8]. The application of paints or anticorrosive paint systems is the most widely used alternative for such[6,9]. However, although it is a comparatively inexpensive and extremely versatile method, it has certain drawbacks, such as the need for good surface preparation and the use of formulations with several different components, some of which may be toxic, as is the case with chromium and lead-based pigments, and hydrocarbon solvents such as toluene and xylene[8-11]. Thus, there is an effort to replace such coatings with non-toxic and environmentally friendly alternatives[12].

Amongst the most current reports found in the literature, the creation of protective barriers using plasma technologies stands out, be it the so-called hot plasma, or the one characterized as cold plasma, in which the substrates temperature remains close to the environmental[13]. In this context, some works use plasma electrolytic oxidation (PEO) techniques[1,2,14,15] and their variants[16,17]; plasma transferred arc (PTA)[18] and thermal spray[19-21], techniques in which the substrate usually reaches high temperatures. Other report deposition processes in low-pressure plasma[5,13,22] and in atmospheric-pressure plasma[22].

Yang et al.[1], coated low carbon steel using PEO in sodium aluminate ($NaAlO_2$) electrolyte, generating coatings composed mainly of alpha alumina (α-Al_2O_3). The results showed that to act as a protective barrier, the micropores present in the coating must be sealed by the molten material that is generated by the deposition process itself. Thus, suitable deposition conditions must be used when it is intended to generate anti-corrosion barriers.

In another study of the same group, carbon steel samples were coated by means of PEO from electrolytes containing different concentrations of hydrated sodium silicate ($Na_2SiO_3 \cdot 9H_2O$). The corrosion resistance of the coatings was analyzed using electrochemical impedance spectroscopy (EIS) and potentiodynamic polarization in a solution containing 3.5% w/w sodium chloride (NaCl). The analyzes showed that the electrolyte concentration has a significant influence on the growth and the protective performance of the amorphous silica (SiO_2) coatings obtained. However, the authors observed the presence of many micropores and

*e-mail: elidiane@sorocaba.unesp.br

cracks in some deposition conditions, which is detrimental for protection against corrosion[15].

Zhang et al.[21] applied a laser re-melting treatment to an amorphous iron-based coating deposited by plasma spray on ASTM 1045 steel. Corrosion resistance was investigated by potentiodynamic polarization in 3.5% w/w NaCl solution. Morphology analyzes showed that the as deposited surface had relatively large pores. However, after the laser melting treatment, a smoother surface was detected, albeit with a fraction of fine microcracks.

Ma et al.[3], deposited a non-crystalline coating resistant to corrosion using PEO in an electrolyte composed of sodium silicate, sodium carbonate, and distilled water on low carbon steel Q235. The results of potentiodynamic polarization tests in NaCl 3.5% w/w demonstrated that there was a 78% reduction in the value of corrosion current density, I_{corr}, in coated steel compared to uncoated steel. However, the authors noted that some deposition conditions generated coatings with the presence of cracks and low adhesion to the substrates.

In another work, Palani et al.[20], investigated the performance of nanocomposite coatings of alumina (Al_2O_3) and titanium dioxide (TiO_2) with different proportions of carbon nanotubes (CNT). Such coatings were deposited on AISI 1020 steel, using the thermal spray technique. After several tests, the authors determined that the optimum mixture was achieved with the proportions by weight of 1% CNT, 88% Al_2O_3, and 11% TiO_2. This proportion guaranteed the best values of hardness and tensile strength. However, the authors did not investigate the corrosion protection properties of such coatings.

Concerning the aforementioned techniques, most of them present as the main disadvantage the fact that the process develops at high temperatures[3,14,16,17], limiting the treatment to heating resistant substrates. Also, the authors frequently report the presence of pores and cracks in PEO deposited coatings[1,3,14], as well as adhesion problems and de-coating of the oxide layer formed on the treated metal[3], characteristics that hinder the protection against corrosion.

In this context, low-pressure plasmas are presented as interesting alternatives for the application of protective coatings, since they allow cleaning processes to be carried out on the metal surface and the treatment of native oxide, as well as the subsequent deposition of films with a wide range of features[23-25]. The process is energetically viable and environmentally friendly, as it requires low power excitation signals and low-pressure atmospheres, thus not generating appreciable residues or atmospheric emissions[24,26,27]. They also allow the application of coatings on substrates of complex shapes, at low temperatures, with high deposition rates and low cost per application[27-29].

Fenili et al.[13] investigated the corrosion resistance of SAE 1020 steel subjected to plasma nitriding and subsequently to deposition of diamond-like carbon film (DLC). The corrosion resistance of the samples was analyzed by electrochemical methods in a 0.1 mol.L^{-1} solution of H_2SO_4. In general, the samples coated with DLC film showed better corrosion resistance than the uncoated samples but the sample that exhibited the best performance was the coated with 1.5 µm DLC film prepared with 500 W of power. However, to ensure the adhesion of the DLC film to the nitrided layer, it was necessary to use an intermediate layer rich in silicon. Also, the authors found that only the nitriding treatment did not result in a protective layer, once it has a porous structure.

In another work, Esbayou et al.[30] deposited organosilicon films using plasma-enhanced chemical vapor deposition (PECVD) from the precursor 1,1,3,3-tetramethyl disiloxane (TMDSO) on carbon steel. The authors studied the influence of different surface pretreatments, which were the amorphous phosphating, the exposure to Ar or N_2 plasmas, on the performance of the obtained coatings. The results demonstrated that the organosilicon films acted as good barriers against corrosion, even after a long time of immersion in the saline environment. However, the sample deposited without a pre-treatment showed low adhesion to the substrate, demonstrating that the pre-treatment is essential for the barrier properties of the coating.

Ma et al.[22] coated J55 and N80 steels, used in oil tubes, with film deposited in plasmas generated from trimethylsilane (TMS). The authors evaluated two deposition methods: atmospheric plasma and low-pressure direct-current plasma. The results showed that the coating generated in the low-pressure plasma is thicker and less porous than that obtained in the atmospheric plasma.

Gangan et al.[31] deposited silicon oxycarbide films on low carbon steel using PECVD with tetraethylorthosilicate (TEOS) as the precursor and argon as the carrier gas. The authors investigated the influence of plasma excitation power on the film corrosion protection properties using potentiodynamic polarization and EIS in 3.5% w/w NaCl solution. The results showed an increase of 98% in the protection efficiency for the sample prepared in 100 W plasma.

Regone et al.[5] investigated the corrosion resistance of commercial carbon steel saws coated with amorphous carbon thin films deposited in plasma. The corrosion resistance of the as received and of the coated saws was investigated using EIS and potentiodynamic polarization in a solution prepared with NaCl and H_2SO_4, with a pH of 3.5. The results demonstrated an increase in the corrosion resistance of two types of carbon steel saws. However, the authors noted that electrolyte penetration still occurs due to the low thickness of the films (~ 1 nm).

Among the coatings deposited in plasma, those deposited from organosilane precursors stand out, whose properties can be adjusted by varying the deposition parameters, thus generating coatings with a composition closer to organic or inorganic. By means of the addition of O_2, or other oxidizing gases in the discharge, it is possible to remove the organic groups present in the precursors and deposit SiO_x-type films, with characteristics like that of silica[32-35]. Among the organosilane precursors most used to prepare such structures is hexamethyldisiloxane (HMDSO) [$(CH_3)_3$-Si-O-Si-$(CH_3)_3$][7,36,37]. Films deposited from HMDSO generally have a cross-linked structure, good adhesion, high deposition rate, and are stable in water[36,38,39].

Silica type films, SiO_x, are often used as protective barriers against corrosion, once they are more inert and denser than organosilicon type films, $SiO_xC_yH_z$. However, organosilicon films have advantages such as greater surface regularity and more flexible networks, which attains physical stability of the structure on different substrates[40].

Santos et al.[40] coated AISI 304 stainless steel with films deposited in plasmas containing 70% HMDSO, 20% O_2, and 10% Ar. It was investigated the effect of the plasma exciting signal on the properties of the coatings. Corrosion resistance was investigated using EIS and potentiodynamic polarization in 3.5% w/w NaCl solution. All the coatings were characterized as an organosilicon, with structures similar to that of the conventional silicone, that is, to the polydimethylsiloxane. According to the authors, the thickness of the film proved to be an important factor for the protection, but the structure of the coating had a predominant effect on the result. It was also suggested that if organosilicon and silica films were interleaved, forming a multilayered structure, a better barrier system could be built, increasing the protection of the coated metal.

Rangel et al.[4] created gradual $SiO_x/SiO_xC_yH_z$ films by PECVD using mixtures of HMDSO, O_2, and Ar and investigated their mechanical and barrier properties. The structural change from organosilicon to silica, and vice versa, was reached only by changing the plasma conditions and without interrupting the process. The corrosion resistance of the films deposited on carbon steel was analyzed using EIS in a 3.5% w/w NaCl solution. The oxidation of the substrate before the deposition of the film enhanced the corrosion resistance of the samples. An increase of around six orders of magnitude in the total resistance, R_t, was detected when the carbon steel was coated, after oxidation, with a gradual 2 µm thick quaternary structure ($SiO_x/SiO_xC_yH_z/SiO_x/SiO_xC_yH_z$).

In another work, Rangel et al.[41] deposited thin films using mixtures of HMDSO and Ar for establishment of the plasmas. The excitation power was varied from 50 to 300 W to change the average energy of the plasma species while the electronic configuration was selected to avoid direct ion bombardment of the films during deposition. The main structural change induced by power variation was related to the proportion of methyl groups that remain attached to the silicon skeleton. The elevation of the film density, ascribed to removal of the methyl groups and to establishment of crosslinkings, resulted in hardness values comparable to that of silica and a structure more resistant to the penetration of oxidative species, whereas preserving the organosilicon nature of the material.

Considering these aspects, the possibility of coating carbon steel with multilayer $SiO_x/SiO_xC_yH_z$ systems that have improved barrier properties was investigated in this work, combining, for their production, deposition, and oxidation methodologies in plasma low- pressure. It was investigated the effect of the oxidation plasma, with the samples in floating potential during the treatment, on the elemental composition, chemical structure, and the corrosion resistance of organosilicon films, deposited in plasma of mixture of hexamethyldisiloxane with oxygen and argon. The corrosion kinetics of the system prepared on carbon steel was investigated by EIS.

2. Experimental

2.1. Substrate cleaning

The plasma thin films were prepared on soda-lime-silica glass substrates, Nylon 6® (polyamide 6, PA-6) and polished AISI 1020 steel. The substrate materials were selected considering the focus of the work and the requirements of the characterization techniques employed. Both the glass and polyamide 6 plates were cleaned using the procedure described by Mancini et al.[42]. The polished carbon steel samples, coated with oil to prevent oxidation, were cleaned immediately before the experiments started. The excess oil was initially removed with paper moistened with isopropyl alcohol. Then, they were cleaned in an ultrasonic bath of isopropyl alcohol for 480 seconds and dried in a hot air stream.

2.2. Experimental apparatus

The cleaned substrates were positioned on the lower electrode of the treatment system illustrated in Figure 1[43]. It consists of a cylindrical glass chamber sealed by two aluminum flanges. A circular stainless-steel screen, connected to the upper flange using rods, and a solid stainless-steel disk, connected to the lower flange, are used as electrodes. Stainless steel tubes allow the admission of gases, coming from the cylinders, in the reactor and their flows are controlled by needle valves (LV-10K, Edwards). The vacuum system consists of a rotary vane pump (E2M18, Edwards) and the system pressure is monitored by a Pirani type meter (APGX, Edwards). The hexamethyldisiloxane monomeric precursor, HMDSO, is housed in a 100 mL borosilicate glass Erlenmeyer, coupled to a needle valve that, like the gases pipes, is linked to stainless steel connections on the upper flange of the reactor. The system is also equipped with a 13.56 MHz radiofrequency (RF) source (RF-300, Tokyo Hy-Power) with variable power

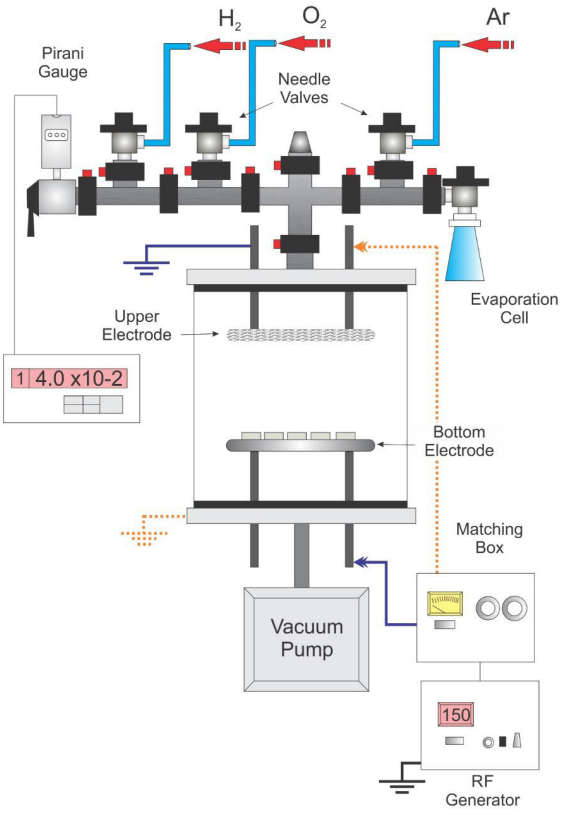

Figure 1. Schematic representation of the plasma treatment system. Electrical configuration (solid line) used in the cleaning treatment and the deposition of the $SiO_xC_yH_z$ film. (Dotted line) Electrical configuration used in oxidation treatments in O_2 plasmas.

from 0 to 300 W. The source can be coupled to the lower electrode (solid line) or upper electrode (dotted line) of the system by an impedance matching circuit (MB-300, Tokyo Hy-Power), which has the purpose of minimizing the reflected signal back to the source.

2.3. Procedures

Before depositing the films, the samples were subjected to a cleaning plasma, composed of hydrogen and argon. This procedure is effective in removing the native oxide from carbon steel, which has a defective and poorly protective structure, in addition to avoiding possible harmful effects of the adhesion of the film to the substrate. For this procedure, the reactor was evacuated until it reached the base pressure (1.6 Pa) when 1.3 Pa of the mixture of 50% Ar and 50% H_2 was admitted, producing a working pressure of 2.9 Pa. The plasma was excited by applying radio frequency signal (13.56 MHz, 150 W) to the lower electrode for 600 s, keeping the upper electrode grounded[29,44].

After the ablation time, the plasma was interrupted as well as the flow of gases. The base pressure of 1.6 Pa was restored to the establishment of the deposition atmosphere composed of 14.0 Pa of HMDSO (70%), 4.0 Pa of O_2 (20%), and 2.0 Pa of Ar (10%) at a working pressure of 21.6 Pa. The plasma was established by applying an RF signal (13.56 MHz, 150 W) to the lower electrode while the upper electrode remained grounded. The deposition procedure was maintained for 1800 seconds.

Finally, the as deposited samples were exposed to the oxidation procedure in O_2 plasma. For that, 3.3 Pa of O_2[45] was admitted in the reactor, stablishing a working pressure of 4.9 Pa. For the treatment to be carried out at floating potential, the lower electrode (sample holder) was kept with no polarization. The plasma excitation signal (13.56 MHz) was applied to the upper electrode, while the reactor walls were grounded. The treatment time was set at 3600 seconds while the power of the discharge generation signal, P, was varied between 10 and 300 W. The effect of this variable on the properties of the films was investigated as described below.

2.4. Characterization procedures

2.4.1. Thickness

The thickness of the as deposited films and of the oxygen plasma treated samples was analyzed by profilometry. The samples were prepared on glass slides containing a mask, also made of glass, over part of its surface area. The system was subjected to deposition, generating a step between the protected and the plasma exposed areas. The step height was determined using a Dektak 150 profilometer (Veeco Instruments Inc.) with 2000 μm scans acquired under 3.0 mg load. Profiles were registered in five different positions of the step and, in each one of them, ten values height were taken, totaling 50 values of thickness per sample. The presented values correspond to the arithmetic mean and the standard deviation of these results. The rate of removal of the layer in the oxidation treatments, R, was calculated using the following formula:

$$R = \frac{(h_f - h_i)}{t} \quad (1)$$

where, h_i is the thickness of the as deposited film, h_f is the thickness of the film after the oxidation treatment and t is the treatment time in minutes.

2.4.2. Chemical structure

The chemical structure of the samples prepared on polyamide 6 were analyzed, before and after the plasma oxidation procedure, by Fourier transform infrared (FTIR) spectroscopy. A Jasco model 410 FTIR equipment was used for that in the ATR mode (MIRacle ™ Single Reflection ATR, PIKE) with a ZnSe crystal and 45º incidence angle. For each sample, 128 scans were performed in the range from 4000 to 520 cm^{-1} with a resolution of 4 cm^{-1}. All spectra were converted to allow comparison with traditional transmittance spectra using the equipment's software.

2.4.3. Elemental composition

Energy dispersive spectroscopy, EDS, was used to determine the elemental composition of samples prepared on carbon steel. A Jeol scanning electron microscope (JSM-6010LA) was used in which a Dry SD Hyper X-ray detector (EX-94410T1L11) with a resolution of 129 to 133 eV for the Mn Kα line at 3000 cps is coupled. To avoid the accumulation of charge on the surface during the inspections, the samples were covered with a thin conductive film prepared by the sputtering process from the target of the Au-Pd alloy. The deposition was carried out with a current of 30 mA for 60 seconds in a metallizer model Desk V, manufactured by Denton Vacuum. EDS spectra were acquired at 2500 x magnifications, using an acceleration voltage of 5.0 kV, with a spot size of 70, which corresponds to a beam diameter of 6.0 nm. Analyzes were performed at five points in each sample and the presented values correspond to the arithmetic mean of these measures. The results were converted into atomic proportions using the equipment's software, which uses the ZAF correction method. The cross-section micrographs were performed on the same equipment, with an acceleration voltage of 2.5 kV, a spot size of 25, and magnifications of 9500x and 25000x. As the inclination of the analyzed samples was not controlled, the layer thicknesses could not be determined by the cross-section analysis[40]. However, qualitative results could be observed.

The surface chemical composition and the chemical state of the detected elements were investigated by X-ray photoelectron spectroscopy, XPS, using a Thermo Scientific model K-Alpha equipment. A source of monochromatic Al Kα radiation was used. The analyzes were carried out on films deposited on glass and, to avoid loading, the electron gun was used. The exploratory scan was performed using pass energy of 200 eV and scan number of 10, while the high-definition spectra were acquired with pass energy of 100 eV, number of scans of 10, and energy step of 0.05 eV. The spot size was 50 μm and the pressure in the analysis chamber was ~ 10^{-9} mbar (10^{-7} Pa). The spectra were analyzed using the Casa XPS 2.3.17 software. The Shirley algorithm

was used to subtract the background and to adjust the peaks while the binding energy scale was calibrated by setting the C 1s peak at 285.0 eV.

2.4.4. Barrier properties

Electrochemical impedance spectroscopy, EIS, was used to evaluate the corrosion resistance of samples prepared on carbon steel. A conventional electrochemical cell with three electrodes and an Autolab potentiostat (PGSTAT 128N) was used. Samples with an exposed area of 1.00 cm^2 were used as the working electrode, while the counter electrode and the reference electrode were made of stainless steel and Ag / AgCl / KCl 3M, respectively. An aqueous solution of sodium chloride 3.5% by weight was used as an electrolyte. EIS measurements were taken in relation to the open circuit potential (OCP) after immersion time of 1800 seconds, with a perturbation signal of 10 mV and varying the frequency in the range of 10^4 to 10^{-2} Hz. The acquisition rate used was 10 points per decade and the test was performed on a sample for each condition (n=1). Appropriate equivalent circuits were used to adjust the results using the ZView software version 3.5b.

3. Results and Discussion

3.1. Chemical structure

Figure 2 shows the infrared spectra of the samples exposed to the oxidation process in plasmas of different excitation powers. The spectrum of the as deposited film and that of commercial polyamide 6 (PA-6) substrate, are also presented.

The bands in the PA-6 spectrum appear around 1540 cm^{-1} (δ N-H and ν C-N)[46-49], 1635 cm^{-1} (ν C=O in amides)[46,47,49], 2866 cm^{-1} (ν C-H in CH_2), 2934 cm^{-1} (ν C-H in CH_2), 3299 cm^{-1} (ν N-H)[46,49,50] and 3080 cm^{-1} (overtone of N-H in 3299 cm^{-1})[47,49]. These contributions are characteristic of the polyamide.

The spectrum of the as deposited sample also presents absorptions related to C-H stretching but shifted in wavenumber from that observed in the PA-6 spectrum. It is known that films polymerized in plasmas containing HMDSO may have a structure similar to that of silicone or polydimethylsiloxane, PDMS, where silicon atoms are surrounded, on average, by 2 oxygen atoms and 2 methyl groups[25,36,45,51].

Thus, the intense absorption peak close to 1020 cm^{-1}, attributed to the stretching of Si-O into Si-O-Si of the skeleton of the siloxane chain[52], is consistent with such a structure. According to Gengenbach et al.[53], the carbon present in films polymerized from HMDSO plasma is predominantly incorporated in the form of methyl groups, as demonstrated by the absorptions related to methyl silyl groups around 790 [δ in Si-$(CH_3)_2$], 850 [ν and δ in Si-$(CH_3)_3$] and 1257 cm^{-1} [ν in Si-$(CH_3)_x$]. The presence of the Si-$(CH_3)_2$ group, considered a chain propagator in the PDMS, is indicative of the formation of long chains of organosilicon material. However, the film does not consist of long and isolated Si-O-Si chains but there is also interchain connections appearing by Si-Si and Si-CH_x crosslinkings[53]. In this structure, the –Si-CH_2-Si- bond should be highlighted because it represents one of the crosslinking points of the long siloxane chains[32,36,51,54]. However, the identification of this group in the infrared spectrum can be hampered by the strong absorption related to siloxane (Si-O-Si) that appears in the same wavenumber, that is, 1020 cm^{-1} [51,55,56]. Other possibilities of crosslinking occur by means of the formation of Si-Si and Si-O-Si bonds. In all cases, the connection presupposes the loss of H atoms or methyl groups.

Finally, there is a small contribution around 3400 cm^{-1} that is attributed to the OH stretching vibration[24,57,58]. Such a band may be due both the moisture adsorbed after the exposure of the film to the environment[59,60] and to the formation of Si-OH groups[59,61,62] during the deposition process.

With the oxidation treatment changes in the spectra of the samples are observed. First, peaks related to the

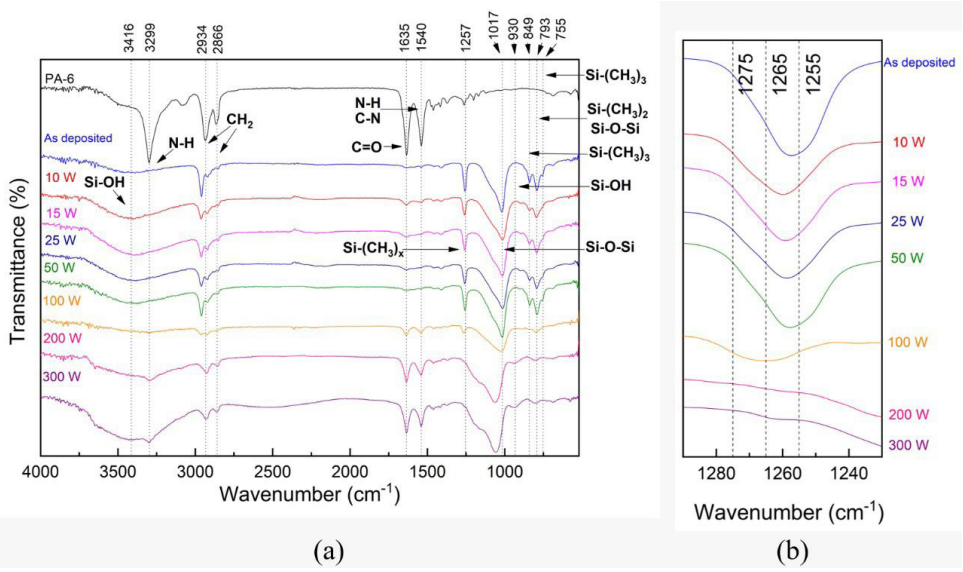

Figure 2. (a) Spectra of transmittance of the substrate (PA-6), of the as deposited film, and the samples treated in oxygen plasmas of different powers. (b) The highlight of the same spectra in the region of the absorption band of the methyl silyl group (1240-1280 cm^{-1}).

substrate groups appear in some of the spectra. This fact is an indicator that the thickness of the layer is being reduced with the increment in the power of the oxidation plasma. According to theoretical predictions[63-65], the infrared beam in ATR mode reaches a few micrometers deep in polymeric materials. As the as deposited film has no peaks related to the substrate, it is estimated that its thickness is greater than 1 μm. For samples oxidized in plasmas of higher power, thicknesses below 1 μm are expected.

With increasing P there is also an enhancement in the intensity of the bands related to hydroxyl groups (3400 cm^{-1}). This contribution may be related to the presence of silanol groups (Si-OH) as well as adsorbed water[32,57,59]. The appearance of a peak at 930 cm^{-1}, related to the deformation of OH in Si-OH, confirms the presence of this group in the treated structure[66] and its possible contribution to the band at 3400 cm^{-1}.

But the main effect produced by the increment of the plasma power is an overall reduction in the intensity of the peaks related to organic groups. A displacement of the peak attributed to the Si-$(CH_3)_x$ group between 1256 and 1265 cm^{-1} is also observed, a fact normally related to the reduction in the number of CH_3 groups linked to the siloxane skeleton[66]. According to Vendemiatti et al.[43] in organosilicon films, silicon of the main chain may be linked to one, two or three methyl groups, producing absorptions at 1275, 1265 and 1255 cm^{-1}, respectively. Thus, the abstraction of methyl groups displaces the peak to larger wavenumbers, as seen in the results in Figure 2b. Besides the displacement, there is a trend to gradually vanishment of this contribution as P is increased beyond 200 W, corroborating the idea of depletion of methyl groups and transformation of the organosilicon layer into silica. The same intensity reduction is observed in the band around 790 cm^{-1} with increasing P once this absorption may have the contribution of organic [Si-$(CH_3)_2$][33] and inorganic (Si-O-Si)[54,58,67] groups.

Therefore, the permanence of this band in the spectra of films in 200 and 300 W plasmas, together with the disappearance of the band related to methyl silyl groups (~ 1260 cm^{-1}), indicate the contribution of the inorganic fraction of the structure (Si-O-Si) to this band and implies in a total conversion of the organosilicon film into a SiO_x type film. For the other samples, the conversion of only superficial layers to silicon oxide and the maintenance of deeper organosilicon may have occurred. This would occur both by the formation of a dense oxide on the organosilicon surface, which would inhibit the action of the treatment in regions below it and by the incomplete removal of methyl groups from the deeper layers. In the case of films completely converted to SiO_x, the dense surface layer was not created and, therefore, the oxidation process was able to convert the entire layer to oxide.

It is also notable the enlargement of the band related to the stretching mode of Si-O groups (~ 1020 cm^{-1}), which can be attributed to chemical changes in the vicinity of the Si-O-Si group[68-71]. According to the literature the position of this peak is related to the stoichiometry of the SiO_x film, being its upwards shift an indicator of the oxidation degree enhancement[32,70,72]. Grill and Neumayer[68] claim that a shift in the frequency of the Si-O asymmetric stretch band indicates a change in the bond angle and that for SiO_2 grown at low temperatures, the peak appears around 1060 cm^{-1}. According to Zajíčková et al.[73] the wavenumber of the Si-O stretching band decreases with increasing film density. The position of this band in the spectra of the as deposited and low power plasma treated samples (<100 W) is the same of the observed in the PDMS spectrum (1010 cm^{-1}), revealing the predominantly organosilicon nature of these samples[72]. In the spectra of the high-power plasma treated films, the peak of siloxane appears in 1025 (100 W), 1061 (200 W), and 1056 cm^{-1} (300 W), moving to larger wavenumbers without, however, reaching the value presented by thermal silica (1090 cm^{-1})[32]. This shift points to a decrease in the density of the films with an increase in the oxidation power despite the transformation of the organosilicon structure into silica.

The band referring to the Si-O stretching mode (1020 cm^{-1}) can provide additional structural information when deconvoluted in its components, as shown in Figure 3a, which shows the spectrum of the sample treated in plasma of 100 W of power.

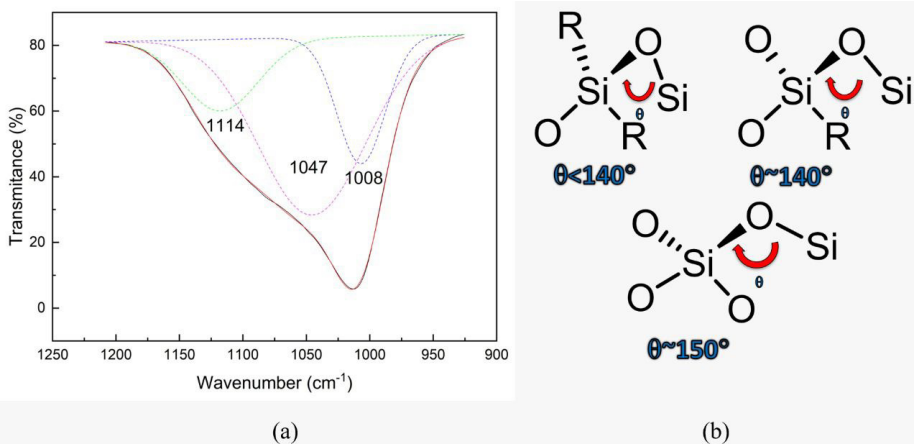

Figure 3. (a) Components of the adjustment of the peak of asymmetric stretching Si-O of the sample treated in plasma of 100 W of power of the excitation signal. (b) Illustration of the Si-O_4 and SiO_x groups, where R = C, Si, and O.

Three components appear centered around 1114, 1047, and 1008 cm^{-1}. In the literature, the component above 1100 cm^{-1} is normally attributed to the SiO_2 bond, in which the Si atom is linked to four O atoms forming an angle of 150°[52,68,74], as schematically illustrated in Figure 3b. This configuration has the structure closest to that of stoichiometric oxide[68,75,76]. The peaks in smaller wavenumbers refer to Si suboxides, that is, Si bound to up to three oxygen atoms forming smaller bonding angles[52,68,74], whose structures are also illustrated in Figure 3b.

Only the untreated and 50 W plasma treated films did not present the component related to tetrahedral oxide, revealing only the presence of silicon suboxides. For all the others, the component related to stoichiometric oxide was identified. An estimative of the density of these groups was obtained by the integrated absorption method[77] using the adjusted components. The results, which were normalized to the unit, are shown in Figure 4 as a function of P. The dotted and dashed lines in this graph represent, respectively, the normalized relative densities of tetrahedral oxide and suboxides for the as deposited film.

There is no evidence of tetrahedral oxide (dotted line) in the as deposited film with the suboxides (dotted line) predominating in the structure. Upon exposure to the plasma, however, there is a tendency towards a decrease in the relative density of suboxides with increasing P and of growth in that of stoichiometric oxide in a complementary way, demonstrating that oxygen treatment is converting one type of structure into another especially at more extreme conditions (200 and 300 W).

Studies in the literature[58,67,73,78,79] show that the content of SiO_4 groups affects the volumetric density of the material due to porosity creation[80]. Furthermore, samples with higher densities of tetrahedral oxide showed greater contribution of the band related to Si-OH (Figure 2a). This trend is confirmed by the relative density of Si-OH groups, depicted in Figure 5 as a function of P, which was calculated by the integrated absorption method from the band at 3400 cm^{-1}.

When the oxidation process is conducted at low powers (10 to 100 W) there is practically no change in the relative density of Si-OH groups with respect to the detected in the as deposited film. For plasmas of higher powers, the relative density of silanol groups increases, quite possibly due to the greater availability of by-products generated during the oxidation process. They recombine with radicals created by abstraction of methyl groups, inhibiting the cross-linking of chains, a factor that also affects the volumetric density of the structure. The same relationship of decreasing in the layer thickness and increasing in the amount of silanol groups was observed by Kondoh et al.[57] when treating organosilicon films in oxygen plasmas. In the present work, films oxidized films in 200 and 300 W plasma present greater contributions of the SiOH and SiO_x groups, which characterizes a film with greater porosity and less density. Nevertheless, the opposite was observed for films oxidized in lower powers plasmas (< 25 W).

Therefore, the analysis of the chemical structure of the samples shows the organosilicon nature of the starting material, with a higher degree of crosslinking than that found in conventional silicone. It is also observed that the oxygen plasma treatment has an oxidative action on the layer when it removes methyl groups and incorporates oxygen and hydroxyl in the created sites. Indications of variation in layer density, induced by oxidation, are also obtained by these analyzes.

3.2. Elemental composition

Figure 6 shows the atomic proportions of C, O, and Si in the films as a function of P, derived from the analysis of XPS (a) and EDS (b). Considering the XPS results, it is noted that the as deposited film (0 W) has 47% C, 24% O, and 29% Si. Conventional silicone ideally has a composition of 50% C, 25% O, and 25% Si. That is, the as deposited film is an organosilicon with a lower C content and, therefore, a more cross-linked structure than the conventional polymer.

Under oxygen plasma treatment, there is loss of C and increase in the proportions of O and Si. The structure is composed of 37% of Si and 61% of O after the oxidation procedure in greater power plasmas, producing a stoichiometry close to that of the silica. That is, the treatment converts the surface into a silicon oxide with C appearing as a contaminant. Even for the treatment in plasma of moderate power (50 W), 37% of Si, 59% of O, and approximately 4% of C are observed.

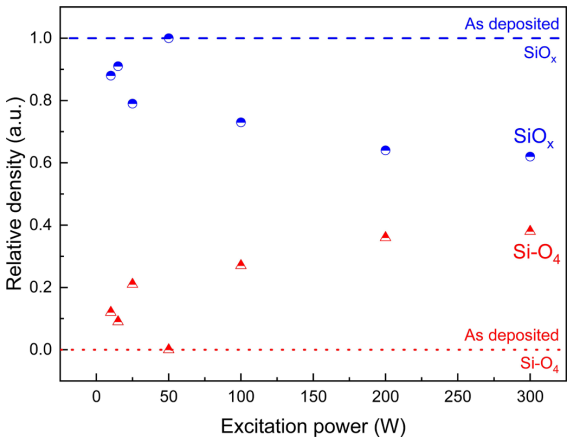

Figure 4. The relative density of $Si\text{-}O_4$ and SiO_x groups ($SiO + SiO_2 + SiO_3$) in the samples as a function of the oxidation plasma power. The corresponding quantities for the as deposited film are represented by the dotted and dashed lines, respectively.

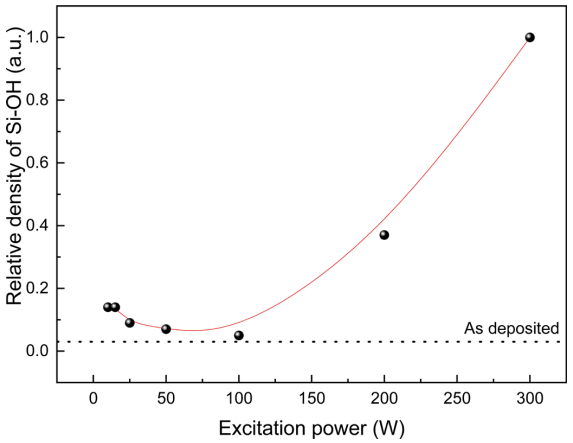

Figure 5. The relative density of Si-OH groups in the samples as a function of the oxidation plasma power. The corresponding quantity for the as deposited film is represented by the dotted line.

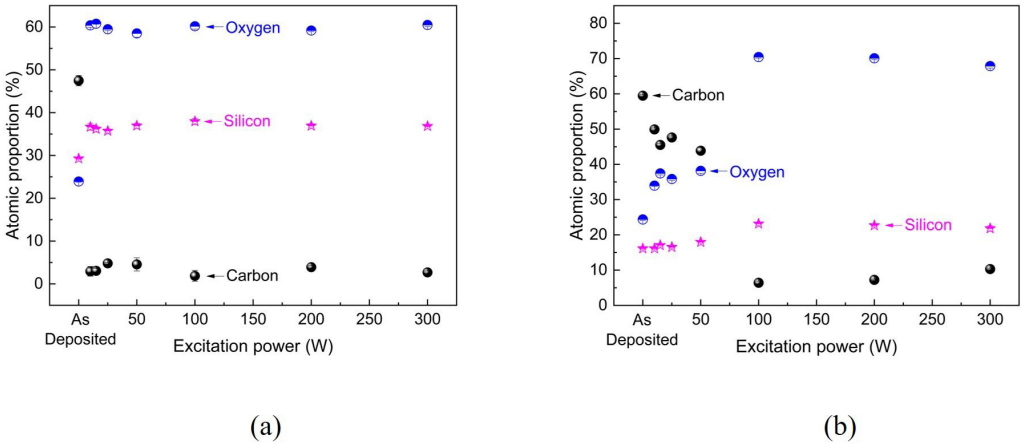

Figure 6. Atomic proportions of C, O, and Si as a function of P derived from analyzes of (a) XPS and (b) EDS.

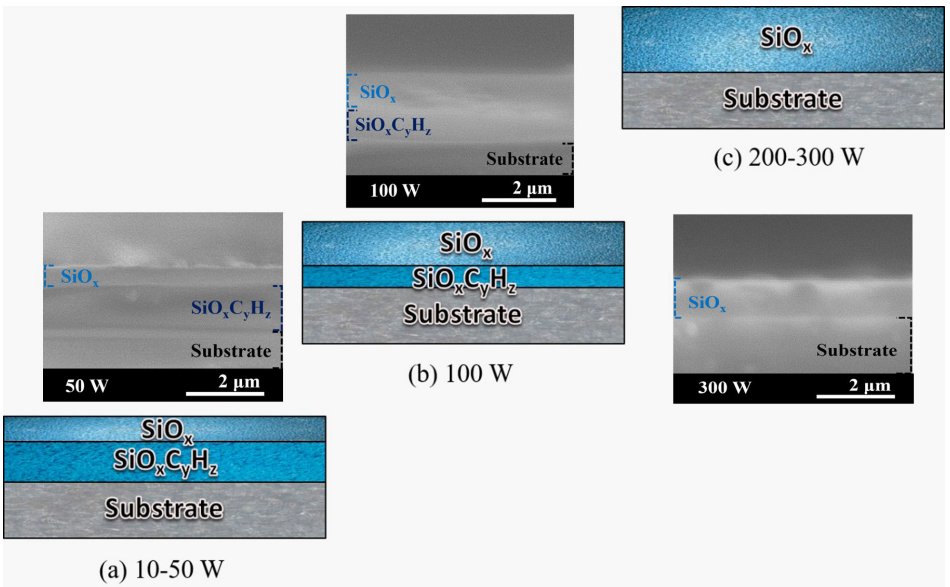

Figure 7. Schematic representation of layer thicknesses, inferred by the union of the results obtained by XPS, EDS, and FTIR, for samples treated with O_2 plasma with powers of (a) 10 to 50 W, (b) 100 W and (c) 200 and 300 W. Scanning electron micrographs of the cross-section of some representative samples (50, 100, and 300 W) are also present.

Thus, the association of XPS (Figure 6a) and EDS (Figure 6b) results, indicates that low power oxidation procedures convert the film surface into an oxide layer but do not change deeper regions whose nature is preserved as organosilicon, as schematically represented in Figure 7a.

According to the EDS results, all samples exposed to plasmas with powers above 50 W can be characterized as oxides. However, infrared spectra, which detect even deeper regions, reveal the presence of organic groups even for samples treated in 100 W plasmas. In other words, although the sample exposed to the 100 W treatment has not been completely converted, there is a substantial increase in the thickness of the converted layer (Figure 7b). The absence of peaks related to organic groups in the infrared spectra of films treated at 200 and 300 W, combined with the results of XPS and EDS, point to the conversion of the entire thickness of these layers into non-stoichiometric oxides (Figure 7c).

Figure 8 shows the high-resolution Si 2p peaks with the components used in the adjustment of the spectra for the as deposited film and for the plasma treated (10, 50 and 300 W) samples. Each component is related to a silicon binding state and the percentage values of each of them, in relation to the total peak area, is presented in Table 1.

The as deposited film shows the Si 2p peak centered on 102 eV, which is in good agreement with the range of position found for the same in the PDMS[37,53]. The adjustment of this peak was performed with 4 components[28,36,66,72,81]. The components at 101.3 and 101.9 eV are assigned, respectively, to the groups $SiO(CH_3)_3$ and $SiO_2(CH_3)_2$[36], while the components at 102.6 and 103.3 eV are due to the $SiO_3(CH_3)$ and SiO_4 groups, respectively[66,82]. The analysis of the percentage areas of the components, in relation to the total peak area (Table 1), shows a predominance of the Si-O_2 bond. This result is consistent with a siloxane structure,

Table 1. Percentage values of the component areas obtained by adjusting the high-resolution Si 2p peaks for the as-deposited film and the samples treated in O_2 plasmas of different powers.

Sample\Component	Si-O_1 (%)	Si-O_2 (%)	Si-O_3 (%)	Si-O_4 (%)	Si-OH (%)
As-deposited	15	62	19	4	---
10 W	---	---	4	47	49
15 W	---	---	4	25	71
25 W	---	---	4	23	73
50 W	---	2	10	7	81
100 W	1	1	---	78	20
200 W	2	---	---	46	52
300 W	1	1	---	52	46

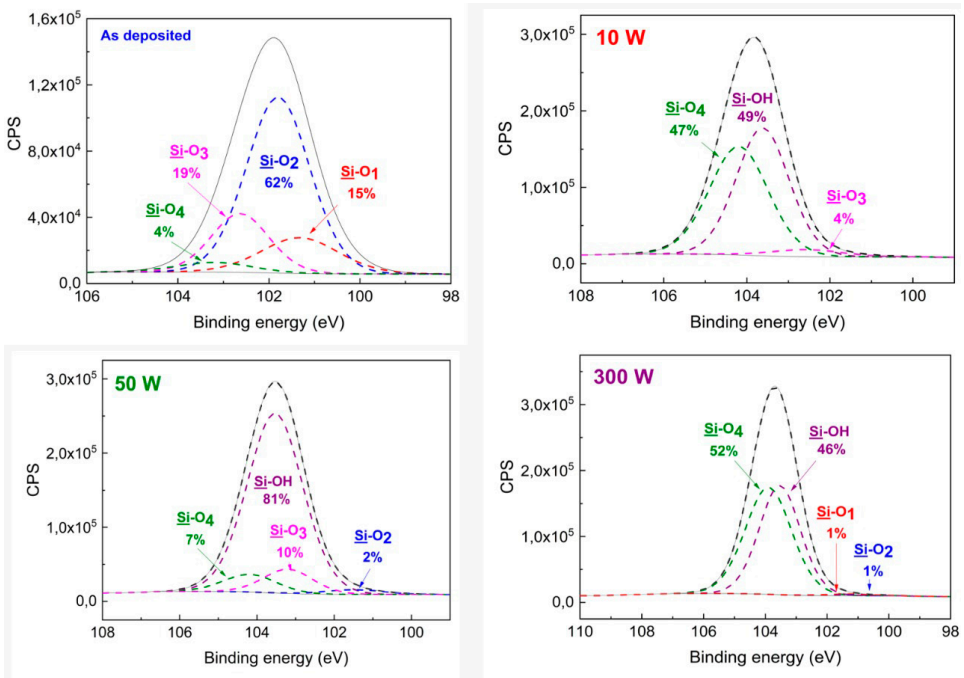

Figure 8. High-resolution Si 2p peaks with the components used in the adjustments. The peaks for the as deposited film and the samples treated in O_2 plasma with powers of 10, 50, and 300 W are present. The percentage values of the area are also present.

as that of the PDMS (Figure 9a) in which the silicon is surrounded by two oxygen atoms and two CH_3 groups, as illustrated in Figure 9b. In this scheme, the Si-CH_2-Si (I), Si-Si (II), and Si-O-Si (III) bonds are highlighted because they represent possible points of connection of adjacent chains in organosilicon films.

For samples exposed to low-power plasmas (10 - 25 W), the Si 2p peak shifts to higher binding energies (~ 103.8 eV) consistently with the range of values of Si in quartz[37]. The number of components required for adjustment decreased to three, which are, 102.6 eV (Si-O_3)[36], 103.6 (Si-OH), and 104.2 (Si-O_4)[83,84], indicating a structure with less variety of chemical environments for silicon.

For films treated in plasmas of greater powers (> 25 W), the suboxides $SiO_2(CH_3)_2$ and/or $SiO(CH_3)_3$ reappear, but in reduced proportions (<3%). In general, the surface can be characterized as a tetrahedral oxide with high proportions of silanol groups, accounting together to more than 90% of the total area of the Si 2p peak.

For treatments conducted in plasmas of powers below 50 W, the absence of suboxides $SiO(CH_3)_3$ and $SiO_2(CH_3)_2$ and the presence of $SiO_3(CH_3)$ together with tetrahedral oxide reveal a conversion mechanism in which methyl groups are replaced by oxygen from the plasma, forming, in smaller proportions, $SiO_3(CH_3)$ ($\leq$ 4%) and, in higher proportions, SiO (20-47%). These changes are accompanied by a substantial growth in the proportion of Si-OH groups. Studies in the literature attribute the incorporation of Si-OH functionals to the silicon oxide[85,86] to the reactivity of the Si-O-Si group, caused by the angle of its bond which allows the repositioning of the π anti-ligand orbital[87,88]. In this way, Si-O-Si groups of the silica react with the moisture of the air to form Si-OH terminals[89,90]. Another phenomenon that may account to this trend is the elevation in the concentration

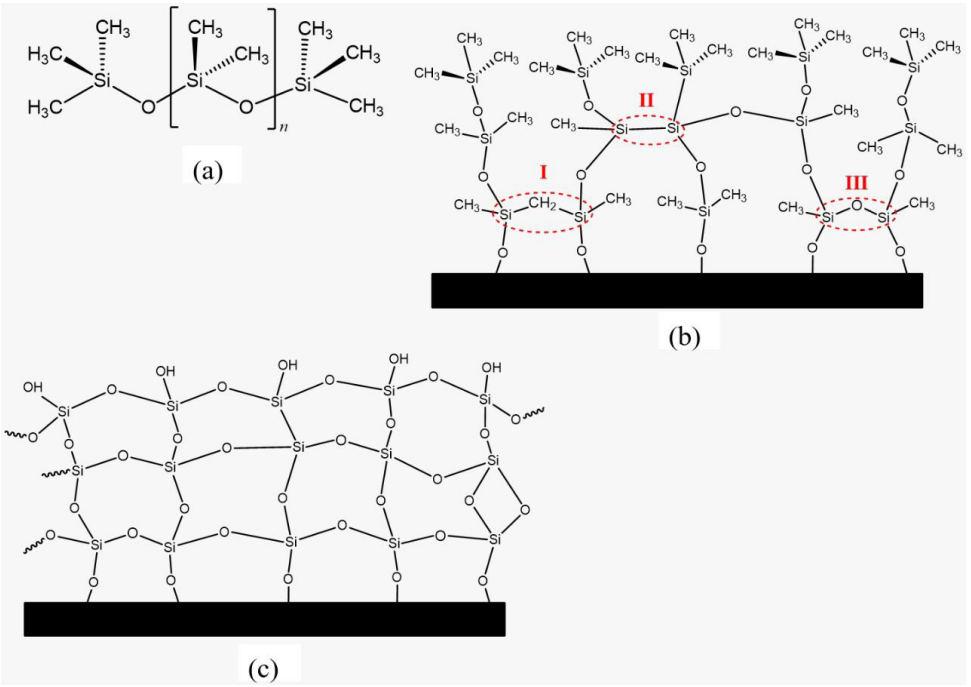

Figure 9. (a) Chemical structure of conventional polydimethylsiloxane, PDMS, where *n* is the number of repetition units; (b) representation of the structure of the plasma polymerized film from a mixture containing HMDSO, O_2, and Ar. (c) Chemical structure of amorphous silicon oxide.

of residual radicals trapped in the structure with increasing P[36]. Pending bonds may react with atmospheric oxygen and water vapor leading to the incorporation of oxygen-containing groups (SiO and SiOH) in the samples[39,60,75,91]. As already mentioned, the oxidation procedure itself is another possible source of incorporation of OH groups in the structure[92].

Important inferences can be obtained from the comparison of the silanol content trends generated from the XPS (Table 1) and FTIR (Figure 5) analyses. Divergent tendencies are noticed for both results, corroborating the idea of a compositional gradient. While the relative density of silanol groups falls with increasing P up to 50 W (Figure 5) for the FTIR results, it grows for the XPS results (Table 1). This analysis allows ones to infer that the increase in the content of silanol groups occurs only on the surface region of the sample. Nevertheless, for treatments conducted with the highest excitation powers, the silanol group is distributed in the overall coating volume.

Therefore, according to the data of Table 1, the highest proportion of suboxides (~ 10%) in the structure was attained for the treatment power of 50 W. The presence of suboxides may favor structural crosslinkings, generating a denser and more compact surface layer. This finding also corroborates the proposal of a surface oxide layer that would protect the deeper organosilicon structure from oxidation, derived from EDS and FTIR analysis.

Another treatment condition that should discussed is the one which resulted in the highest proportion of tetrahedral oxide groups (78%) and the lowest proportion of suboxides (~ 2%), that is, 100 W. In this sample, the reduced proportion of silanol groups is ascribed to the low availability of radicals trapped in the structure due to an efficient saturation of pendant bonds by oxygen of the plasma. However, the saturation of radicals with the incorporation of O (SiO_4) inhibits crosslinking. According to previous results, there is suggestion that the thickness of the oxidized layer grows with P and, although the conversion does not reach the entire film layer, 100 W of power is considered the condition that best converts the organosilicon surface into tetrahedral oxide. According to reports in the literature, the XPS error value is typically 2-4%, and for very weak signals this value can reach 8-10%[53]. For a conservative estimate, an error of 15% was considered. Although the presence of some SiO species is within the uncertainty range of the analysis methodology, if these components had not been inserted during the adjustment of the peaks, the fitting would not converge. For this reason, such components were considered to be contaminants.

According to the previous discussion, there is a close relation between the proportion of Si-OH groups and of tetrahedral sites (SiO_4), once the latter define the proportion of residual free radicals left in the structure. The presence of suboxides, on the other hand, seems to correlate with increases in density as they enable the crosslinking of siloxane chains[32,36,51,54].

The type of Si-O-Si structure created from oxidation also justifies the proportion of silanol groups and the density of the resulting material. Together with the FTIR results, the highest concentration of Si-OH on the surface of the sample treated in 50 W plasmas, indicates that this coating has a network-like structure, similar to that of SiO_2. It is known that such a structure favors the densification of the material[79] for presenting a high degree of crosslinking[52,68]. On the other hand, the lower proportion of Si-OH on the surfaces treated

with power above 50 W, indicates a cage-like structure, in which the angle of the Si-O-Si bond is different and is not so favorable to incorporation of silanol terminals[89] as the previous one. The cage-like structure culminates in a lower degree of cross-linking and greater porosity[68].

Therefore, the association of results obtained from elemental composition and chemical structure show that the organosilicon layer is converted into a non-stoichiometric oxide with a thickness dependent on the plasma power. The absence of absorptions due to C containing groups in the infrared spectra of samples treated in higher power plasmas (> 100 W) suggests the total conversion of the layer into a porous oxide. The conversion of only a fraction of the layer into oxide was also proven for treatments with moderate powers (10-100 W), generating a $SiO_x/SiO_xC_yH_z$ bilayer. The analysis of the high-resolution Si 2p peaks indicates that plasma power influences not only the thickness of the converted layer but also the degree of conversion.

3.3. Layer Thickness and Material Removal Mechanisms

Figure 10 shows the layer thickness, h, and the material removal rate, R, as a function of P. The thickness of the as deposited film, represented by the range of values between the dotted lines, is around 1.5 μm in good agreement with literature reports for the same type of material[29,43]. For treatments conducted in low-power plasmas (< 50 W), no significant variation in thickness is observed. However, a clear downward trend appears for treatments performed with powers above 25 W.

These behaviors are ascribed to the species removal mechanism be dependent on the plasma excitation power, as evidenced by the variations in the R curve of Figure 10. The rate of material removal is progressively increased with the elevation of P above 25 W.

In addition to altering the molecular structure of the films by removing hydrogen, carbon, and methyl groups, etching in oxygen plasma[45,57,60,83,92] can also be pointed out as the mechanism responsible for the thickness variations detected in the graph of Figure 10. It is postulated that the removal of elements from the layer occurs mainly by the action of oxygen and O_2^+ ions, as verified by Granier et al.[45]. In glow

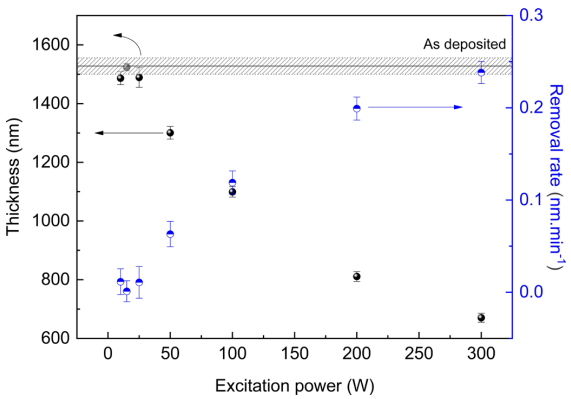

Figure 10. Layer thickness and material removal rate as a function of the oxidation plasma power. The range of thickness values of the as deposited film is represented between the dotted lines.

discharges generated from O_2, the most likely activated species are O, O_2^+, and O^+ generated by the reactions[93]:

$$O_2 + e^- \rightarrow O + O + e \quad (2)$$

$$O_2 + e^- \rightarrow O_2^+ + 2e^- \quad (3)$$

$$O + e^- \rightarrow O^+ + 2e^- \quad (4)$$

The energy required to break the bond between two oxygen (reaction 2) is approximately 4.5 eV, while the energy required for the ionization of O_2 (reaction 3) is approximately 12.2 eV. For the ionization of atomic oxygen (reaction 4), approximately 13.1 eV[93]. Considering that the average electron temperature in discharges of this type does not exceed 5.0 eV[93,94], reaction 1 is expected to be the predominant one. This analysis supports the idea that the main agent responsible for the removal of organic groups from organosilicon layers is atomic oxygen. In general, atomic oxygen has the function of creating reactive points where O_2 chemisorption can occur[94].

The elevation in the plasma excitation power promotes a rise in the average electrons energy and/or density. These physical changes straightly affect the plasma chemistry: the density of atomic oxygen tends to enhance explaining higher oxidation efficiencies for higher P values[29,95]. In the work of Granier et al.[45], it was observed, by X-ray reflectance analysis, a 38% decrease in the layer thickness for oxidation process conducted in 300 W plasma. In the present study, for the same power condition, a reduction of approximately 56% was observed. However, it should be noted that in the system used by Granier et al.[45] the samples were placed outside the plasma creation zone, differently from the present case, what justifies the higher rate of material removal.

SiO_2 layers are known to be resistant to etching in O_2 plasmas[29,92,96]. This means that the formation of a homogeneous and dense layer of SiO_2 on the top of the organosilicon film would interrupt the oxidation of organosilicon structure underneath the surface. In this situation no substantial changes would be promoted in the layer thickness, as observed in the lower power plasma treatments. However, variations in the material removal rate and layer thickness for P > 25 W show that etching is not interrupted in these situations, but instead, it is accentuated. This is also confirmed by the complete transformation of the organosilicon structure into oxide, demonstrated by the infrared spectra of the samples treated in plasmas of greater powers (Figure 2a). A process that would explain variations in film thickness with increasing P would be the removal of material by the sputtering process. Kondoh et al.[57] declare the existence of a competition between the formation and the removal of the SiO_2 layer by sputtering. As in the present work the samples were treated in floating potential, it is postulated that the contribution of sputtering during oxidation is negligible. Another possibility is that, as indicated by the analysis of the chemical structure of the films, the oxidized layer is not dense enough and allows the diffusion of oxidative species

to regions beyond those already altered. In this situation, the diffusion of the active plasma species through porous oxide would explain the oxidation in deeper regions as well as variations in layer thickness.

Considering the oxidation mechanisms, the removal of methyl groups by etching and the incorporation of oxygen in the structure are pointed out as the essential mechanisms for transforming the organosilicon structure into oxide. Some of the ways for such conversion are proposed in reactions 5 to 8[92]:

$$-Si-CH_3 + O \rightarrow -Si-H+O=CH_2 \quad (5)$$

$$-Si-H+O \rightarrow -Si\bullet + \bullet OH \quad (6)$$

$$-Si\bullet + \bullet OH \rightarrow -Si-OH \ ou \ -Si\bullet + O \rightarrow -Si-O\bullet \quad (7)$$

$$-Si-O\bullet + \bullet Si- \rightarrow -Si-O-Si- \ ou \ -Si-O\bullet + H^+ \rightarrow -Si-OH \quad (8)$$

In reaction 5 a terminal methyl group reacts with atomic oxygen and a methylene group (CH_2) is released[62,92], resulting in the formation of silane and formaldehyde ($O=CH_2$). This by-product, whose formation has already been confirmed by van Hest et al.[92] in oxidation plasmas, generates CO, CO_2, and H_2O when recombining with oxygen, an abundant species in the plasma. In general, oxidized by-products are removed from the system by the vacuum pump[25,92,96,97]. The silane group, which replaces the terminal methyl, may then react with atomic oxygen (reaction 6) to form a hydroxyl and a free radical in the chain. The resulting hydroxyl may combine again with the free radical to form a silanol group (Si-OH)[62,92] or allow the radical to follow the mechanism proposed in Equation 7, in which it reacts with another atomic oxygen generating Si-O, with one valence electron remaining in the oxygen. This may bind to another free radical forming the –Si-O-Si- bridge, characteristic of silicas[36,45,52], react with hydrogen present in the glow discharge also forming a silanol, as shown in Equation 8[92], or still keep in the structure as a pendant bond. Considering all these possibilities for the results discussed in the present work, it is inferred that the main mechanism of Si saturation in reaction 6 and 7 is the incorporation of atomic oxygen since siloxane groups have been found in the infrared spectra while silane functional (2100 and 950 cm^{-1}) has not been observed. These mechanisms also explain the formation of Si-OH and the existence of active free radical trapped in the film structure.

According to Clergereaux et al.[83], Si-H and Si-OH, and $Si-CH_3$ are terminal groups straightly related to the density of the films. The removal of these groups affects the density of the material as it allows the formation of crosslinking[29,36,52,83]. Also, amongst these terminals, the methyl group is the densest one[98] and therefore, its substitution by Si-H or Si-OH, results in a more open structure, facilitating the permeation of species, a factor that explains the continuity of the oxidation process with the formation of the oxide on the surface. This mechanism of incomplete oxidation (Si-OH and Si-H) of the structure explains the action of the plasma over the entire thickness of the layer.

From these reports, it becomes evident that the density of the oxidized layer is dependent on the plasma oxidation mechanisms which, in turn, are dependent on P. For lower power plasmas, the constancy in the layer thickness along with the growth in the proportion of tetrahedral oxide (SiO_4) and of silanol groups (Table 1) are indicators of an incomplete oxidation process. For plasmas with moderate powers (50-100 W), as the process is conducted more quickly, compared to the previous one, oxidation is more effective. There is an increase in the removal of organics, the incorporation of oxygen, and the generation of residual radicals favoring cross-linking, and reducing the structure porosity. The preservation of the organosilicon layer underneath the top oxide layer generates a multilayered system. When high power plasmas are used, a porous suboxide is formed, due to the rapid saturation of radicals by oxygen and hydroxyls throughout the volume of the film and not only on its surface. There is formation of a less reticulated network that favors the permeation of oxidative species and the continuity of the process in deeper layers, inducing the creation of a uniform layer of porous oxide. Therefore, considering that the target of this work is to create films to furnish improved barrier properties to metallic substrates, the oxidation in plasmas of moderate powers (50 W) would be the most appropriate condition since it does not produce a porous oxide and does not affect the layer thickness. Energetic reasons also support such a choice.

3.4. Barrier Properties

Figure 11 shows the phase angle as a function of the frequency of the perturbation signal, obtained from samples prepared on carbon steel by EIS. The different curves represent the phase angle of the systems containing the as deposited film and those exposed to the oxidation treatments in plasmas of different powers. The corresponding result for uncoated carbon steel is also presented.

Considering the as received carbon steel, is noticed a typical curve with one time constant and maximum (70°)

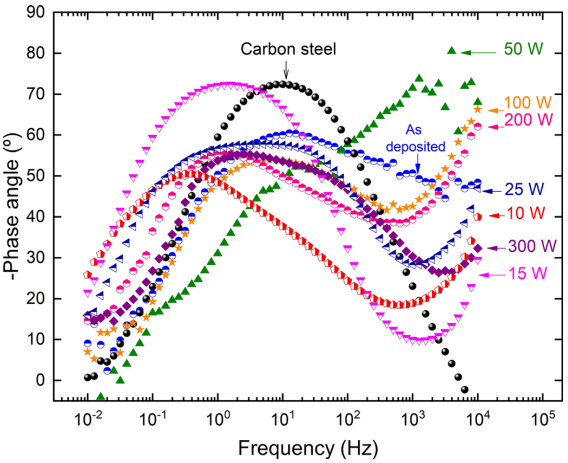

Figure 11. Phase angle as a function of frequency for carbon steel without coating and coated with organosilicon film as deposited and treated in oxygen plasma of different powers. Results obtained in 3.5% NaCl solution (w/w).

around 10^1 Hz, representative of the interactions between the electrolyte and the substrate[24,29,99]. When the phase angle is measured in the carbon steel coated with the as deposited organosilicon film, the end of the curve at high frequencies moves to greater phase angles. This upward displacement suggests a layer with capacitive effect on the electrical circuit, producing a 50° dephasage between voltage and current. In ideally capacitive systems, this shifting would be of 90°, so that the closer to this value, the greater the opposition of the film to the electrolyte charge flow[29,39,66].

In the curves of samples oxidized in plasmas of 10 and 15 W, two time constants appear: one, at low frequencies (10^{-1}-10^0 Hz), which reveals interactions of the electrolyte with the metallic surface, and the other, at high frequencies (10^3-10^4 Hz), which indicates the interactions between the electrolyte and the film. The phase angle at the highest frequency is lower than in the system containing the as deposited organosilicon film, indicating deterioration of the barrier properties in these treatment conditions. However, with increasing the power of the oxidation plasma beyond 15 W produces an elevation tendency in the high frequency edge, reaching about 70° for samples treated in 50-100 W plasmas.

For the sample exposed to the 50 W plasma, the elevation of the phase angle at high frequency, together with the smoothing of the second time constant, suggests less contribution of the processes that occur at the metallic interface[29,39,66] and, therefore, a structure that offers greater resistance to the permeation of the electrolyte species. For this sample, the phase angle value at the high frequency end was higher than that obtained in the system containing the as deposited organosilicon film.

Despite the inorganic film furnishes a better protection against corrosion than the organosilicon one, its physical stability is inferior[26,67,100]. Thus, the bilayers (organosilicon/SiO_x) may improve the barrier properties of the system by combining the good physical stability of the organosilicon with the good barrier of the oxide[67,100,101]. Although the sample exposed to the 100 W plasma also showed a high phase angle (70°), the drop in intermediate frequencies and the presence of a second well-defined time constant indicate penetration of the electrolyte and increase in electrolyte-substrate interactions.

Finally, the phase angle, at high and intermediate frequencies, falls again with an increase in P beyond 100 W, consistently with the drop in layer thickness and the formation of a porous structure of silicon oxide. Therefore, as one concerns the phase angle results, the optimum oxidation condition is considered to be 50 W since it induces the creation of a dense suboxide layer that preserves the underneath organosilicon layer. As both the organosilicon and the oxide represent barriers against permeation of species, a thinner bilayer system but more efficient to inhibit corrosion than the uniform as deposited organosilicon layer is created.

Figure 12 shows the results of the impedance module, |Z|, as a function of the frequency for the samples investigated here, obtained by EIS.

In general, there is a drop in the impedance of the samples with the increase in the frequency of the perturbation signal, typical behavior of these systems[25,29,39,66,99]. Besides, it is noted that the curves are distributed in different positions along the impedance axis. The lowest curve represents the impedance variations with frequency for the uncoated carbon steel. The systems containing the as deposited organosilicon film and the film oxidized in 50 W plasmas resulted in the highest curves. All the other samples showed curves at intermediate heights between those of carbon steel and of the system containing the film treated in 50 W plasmas.

Specifically, it is noted that the power of the oxidation plasma affects |Z| in different ways, that is, there are oxidation conditions that increase the impedance of the organosilicon layer while others decrease it.

The impedance module at low frequencies (10^{-1} Hz) is associated to the total resistance of the system to the current flow, R_T. The higher the R_T the greater the system's opposition to the flow of oxidative species from the electrolyte, that is, the better the barrier property of the film[25,29,39,66,99]. The R_T values were determined according to the method proposed by Mansfeld[29,71] and are depicted in Figure 13.

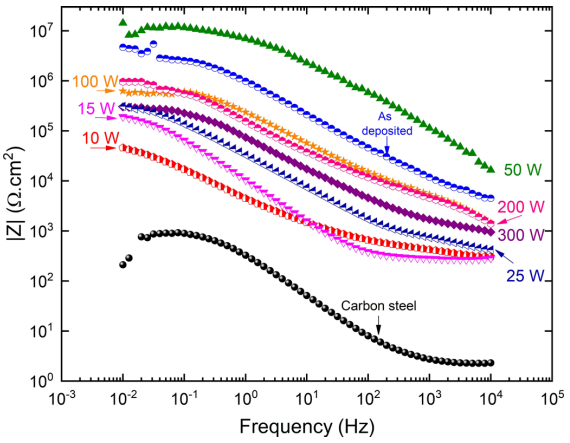

Figure 12. Impedance module as a function of frequency for carbon steel without coating and coated with organosilicon film as deposited and treated in oxygen plasma of different powers. Results obtained in 3.5% NaCl solution (w/w).

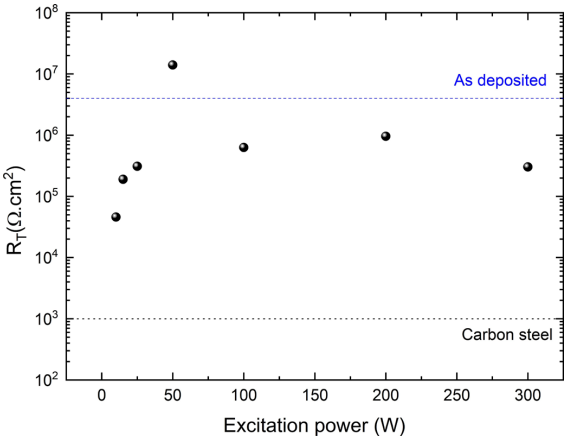

Figure 13. The total resistance of the systems as a function of the oxidation plasma power. The equivalent result for carbon steel as received (dotted line) and that coated with organosilicon film (dashed line) are also presented.

It is possible to observe that the as-received carbon steel has an R_T of the order of 10^3 Ω.cm^2. In the system containing the organosilicon film (as deposited), $R_T = 4.0 \times 10^6$ Ω.cm^2, that is, 1000 times greater than that for the uncoated carbon steel. This demonstrates that the organosilicon layer substantially inhibits the permeation of species from the electrolyte to the metallic interface, representing a barrier against the permeation of species.

It is interesting to observe, however, the trend inversions in R_T with P variations. For the organosilicon layer treated in plasma of 10 W of power, R_T is reduced about 100 times with respect to the value obtained for the as deposited organosilicon (4.0×10^6 Ω.cm^2). Although the thickness of the layer has remained unchanged, the incomplete conversion of surface layers produces losses in the barrier properties. This result corroborates the interpretation that the oxide layer generated on the surface in these conditions is not dense. However, increasing the power of the oxidation plasma between 10 and 50 W causes R_T to grow continuously reaching 1.4×10^7 Ω.cm^2, exceeding the value obtained for the system containing the as deposited organosilicon film (4.0×10^6 Ω.cm^2). In other words, under specific conditions, the organosilicon surface oxidation process, which converts only a small fraction of the layer to silicon oxide, creates a bilayer film that benefits the barrier properties of the system even with a reduction in its thickness. This result is another indication that the oxidation process generates, in this condition (50 W), a denser oxide layer that inhibits the action of the plasma in the layers below as well as the permeation of oxidative species to the metallic interface. Finally, when P is elevated beyond 50 W, a further drop is observed in R_T indicating the deterioration of the barrier properties both by the drop of the layer thickness and by the formation of a completely oxidized, but porous layer. It is noteworthy that the results obtained for carbon steel, organosilicone film, and silicon oxide type (200 and 300 W) are similar to those found in other studies[4,29,41], ensuring the reliability of the analyses, although they were performed once for each condition. With these results, it can be inferred that the degree of crosslinking of the structure, together with the layer thickness, are the most relevant factors to inhibit the flow of species further than its stoichiometry.

The data obtained using the EIS technique can be adjusted to a theoretical model of an equivalent circuit (EC), which allows discerning the contribution of each element of the coating-substrate system to the obtained values[24,26,66,99].

The two equivalent circuits shown in Figure 14 were used to adjust the EIS data of the uncoated carbon steel and of the coated carbon steels with the as-deposited and the O_2 plasma-treated films at different powers, respectively.

The equivalent circuit model shown in Figure 14a represents the electrochemical corrosion process for uncoated carbon steel. The double electrical layer formed on the metal surface has electrical properties similar to those of a simple electrical circuit composed of two resistors and a capacitor[102]. In this model, resistor Rs represents the resistance of the electrolyte between the working electrode (uncoated steel) and the counter electrode[24,26,99]. The resistor Rct, in turn, is related to the resistance of charge transfer on the metal surface[24,66,99]. This charge transfer is nothing more than the transfer of electrons from an anodic region to a cathodic region on the metal surface that occurs in the corrosion process[26,66]. Thus, the charge transfer resistance value is a good indicator of the corrosion resistance of the investigated system[102]. Finally, the charge separation in the double electrical layer can be adjusted using a capacitor, Cdl.

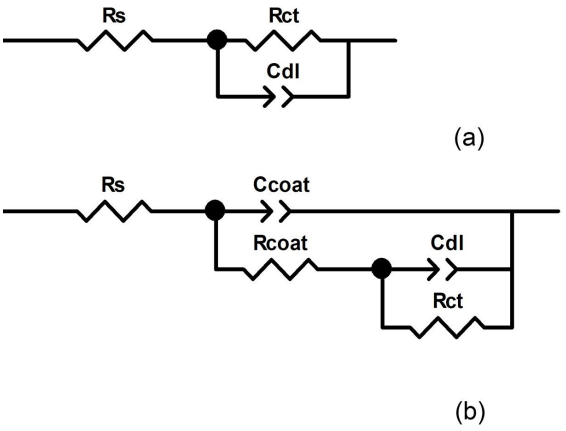

Figure 14. Equivalent circuits were used to adjust the EIS results for (a) carbon steel without coating and (b) carbon steel coated with the as deposited film and films treated with O_2 plasma at different powers.

For solid electrodes, the value of the capacitance of the double electrical layer is usually considered to be affected by imperfections and heterogeneities on the metal surface. In this way, for a more precise adjustment, this effect is simulated using a constant phase element (CPE)[61,62,99]. According to Sun et al.[99], the constant phase element does not have a specific physical meaning and can be defined as follows:

$$Z_{CPE} = \frac{1}{T(j\omega)^{\alpha}} \quad (9)$$

Where α and T are independent of the frequency ω; $j = \sqrt{-1}$ and the exponent α varies from 0 to 1. When α = 1, T represents the capacitance of the metal-electrolyte interface and has capacitance unit. When α = 0, Equation 9 represents a pure resistor and the corresponding resistance can be calculated[26,62,99].

A capacitor takes time to reach its full charge, which produces a lag between the current and voltage in the phase angle curves (Figure 11)[102]. Thus, observing the phase angle curve for uncoated carbon steel, it is possible to notice that it presents only a lag, or time constant, which is properly adjusted by the Cdl capacitor modified by the constant phase element[61,66].

The application of a coating on the metal generates a second time constant[102]. In this way, the electrochemical corrosion process for coated carbon steel samples can be modeled using the equivalent circuit shown in Figure 14b. This circuit is commonly used for simulations of substrates with barrier coatings[24,61,103]. In this circuit, in addition to the elements present in the previous circuit due to the interaction between the metal interface and the electrolyte (Rct and Cdl) and the resistance of the solution (RS), a resistor element, Rcoat, appears, representing the resistance of the coating

Table 2. Element values for the equivalent circuit models of uncoated carbon steel, as deposited film, and samples treated with O_2 plasmas of different powers.

Sample	Rs ($\Omega.cm^2$)	Rcoat ($\Omega.cm^2$)	Ccoat-T ($F\ cm^{-2}$)	Ccoat-α	Rct ($\Omega.cm^2$)	Cdl-T ($F\ cm^{-2}$)	Cdl-α
Carbon steel	2.31	---	---	---	$1.09x10^3$	$5.86x10^{-4}$	0.847
As deposited	2865	$8.22x10^4$	$1.44x10^{-7}$	0.743	$3.31x10^6$	$8.44x10^{-8}$	0.726
10 W	402.6	$4.56x10^3$	$1.30x10^{-5}$	0.620	$6.99x10^4$	$3.37x10^{-6}$	0.770
15 W	249.7	$1.77x10^2$	$2.29x10^{-6}$	0.816	$2.25x10^5$	$6.66x10^{-7}$	0.909
25 W	483	$2.45x10^4$	$1.75x10^{-6}$	0.681	$4.18x10^5$	$1.49x10^{-10}$	0.894
50 W	1456	$7.36x10^5$	$5.25x10^{-9}$	0.839	$1.24x10^7$	$2.63x10^{-8}$	0.572
100 W	723.3	$1.18x10^4$	$2.77x10^{-7}$	0.727	$8.27x10^5$	$7.24x10^{-7}$	0.688
200 W	364.2	$1.09x10^4$	$5.13x10^{-7}$	0.662	$1.51x10^6$	$1.28x10^{-6}$	0.673
300 W	989.7	$1.67x10^4$	$2.37x10^{-6}$	0.698	$3.60x10^5$	$1.05x10^{-6}$	0.727

Table 3. Percentage error values for each element and goodness of fit ($\chi 2$) values.

Sample	Rs Error (%)	Rcoat Error (%)	Ccoat-T Error (%)	Ccoat-α Error (%)	Rct Error (%)	Cdl-T Error (%)	Cdl-α Error (%)	GoF (χ^2)
Carbon steel	1.5	---	---	---	1.9	1.5	0.4	4.4×10^{-4}
As deposited	4	2.6	4.2	4.3	3.2	0.8	0.6	$2.91x10^{-5}$
10 W	2	3.7	1.1	0.4	2.6	2.3	2.2	$1.19x10^{-4}$
15 W	1	1.8	0.4	2.1	0.5	0.2	0.6	$4.19x10^{-6}$
25 W	2	14.6	0.4	0.5	2.2	15	6.7	$7.73x10^{-5}$
50 W	9.3	5.8	3.2	2.3	8.9	3	4.8	$4.20x10^{-4}$
100 W	8	2.9	2.7	2.8	4.9	4	14.2	$2.70x10^{-4}$
200 W	17	3.4	3.9	3.3	12.9	3.2	10.9	$7.07x10^{-4}$
300 W	2	9.6	2.6	1.3	7	4.7	3.3	$7.39x10^{-4}$

together with a capacitor element, Ccoat, representing the capacitance of the coating.

With the proper adjustment using the equivalent circuit models, it is possible to obtain the values of the circuit elements. Table 2 lists the values of the elements of the equivalent circuits used in the adjustment for carbon steel without coating, coated with the as deposited film, and those treated with O_2 plasmas of different powers. Table 3 shows the percentage error values for each element and also the goodness of fit values, represented by $\chi 2$.

According to Sun et al.[99], $\chi 2$ values in the range of 0.003 to 0.01 are adequate for a good fit, so that the values obtained are acceptable.

The total resistance values obtained by analyzing the impedance module at low frequencies, which are depicted in the graph in Figure 12, represent the sum of all the resistances in the system[25]. Analyzing the values of Rcoat and Rct it is observed, in general, that those associated with the last component have a greater impact on the value of the total resistance of the system. This is because Rct is associated with phenomena on the metal surface[26,66,104], so that changes in the barrier properties of the coating will culminate significant changes in the value of this element. According to Fracassi et al.[26], the resistance to charge transfer, Rct, is related to the inhibition capacity of SiO_x coatings.

On the other hand, the coating resistance element, Rcoat, is also known as pore resistance[25,99,102,104],because it is the resistance offered to the penetration of the electrolyte in pores of the coating or areas where greater absorption occurs, due to pre-existing defects or porous areas with inadequate polymer entanglement[104]. In this context, it can be observed that the as deposited film has a high Rcoat value ($8.22 \times 10^4\ \Omega.cm^2$). The cross-linked and highly branched structure of the organosilicon film presents difficult paths for the electrolyte species. On the other hand, for films treated in O_2 plasma with 10 and 15 W, there is a sharp drop in Rcoat compared to the value obtained for the as deposited film. This seems to indicate a degradation of the barrier properties of the organosilicon film, thus generating a coating with permeation paths more easily accessible for the electrolyte species. However, an increase in the plasma power to 25 and 50 W causes the Rcoat to rise to $\sim 10^5\ \Omega.cm^2$, which indicates a more compact oxide-like structure. In the curves of samples treated with powers greater than 50 W, there is a further drop in the values of Rcoat. It is interesting to note that, for the sample treated in 50 W plasma, which had the highest total resistance, the Rcoat value is also higher than that of the as deposited film, indicating a structure capable of suppressing, more efficiently, the absorption of electrolyte's water.

The presented results indicate improvements in the performance of the system against corrosion by the deposition of the organosilicon layer. The oxidation process did not bring any advantage when performed in low (10 to 25 W) and in high (100 to 300 W) energy conditions. However, under moderate energy conditions (50 W), the results point to the creation of a bilayer system with greater resistance to electrochemical attack than the organosilicon layer, even though its thickness is lesser than this. These results corroborate the interpretations proposed in the analysis of the chemical structure and elemental composition of the samples

and are in good agreement with those of the electrochemical impedance spectroscopy.

4. Conclusions

Organosilicon films, with thicknesses of about 1 μm, were uniformly deposited on the surface of the carbon steel, glass, and polyamide. The post-deposition treatment with O_2 plasma causes the removal of methyl, carbon, and hydrogen groups and the incorporation of oxygen in the reactive sites, transforming the treated region into oxide. The degree of conversion and the density of the resulting silica was observed to depend on P. Treatments with low and moderate powers (10 to 100 W) resulted in $SiO_x/SiO_xC_yH_z$ bilayer systems, while those with high powers (200 to 300 W) promoted the complete conversion of the organosilicon layer to silica. In other words, it is possible to control the degree of oxidation of the organosilicon film just by varying the excitation power of the O_2 plasma. The corrosion resistance of the system prepared on carbon steel was observed to depend on the final layer thickness and on the connectivity of the structure converted to silica rather than on the thickness of the converted layer. The treatment condition chosen as optimal in this work was that conducted with 50 W of power due to the creation of a thin, compact inorganic surface layer, with a surface structure similar to that of silica, in addition to preserving the thickness of the film and increasing the barrier properties of the system.

Acknowledgments

This study was financed in part by the Coordenação de Aperfeiçoamento de Pessoal de Nível Superior - Brasil (CAPES) - Finance Code 001. The authors would like to thank LMN / LNNano / CNPEM (Campinas-SP, Brazil) for the use of XPS, XPS Thermo Scientific K-Alpha. And also, to CAPES (1560670) and FAPESP (2017/21034-1) for financial support.

References

1. Yang W, Li Q, Liu W, Liang J, Peng Z, Liu B. Characterization and properties of plasma electrolytic oxidation coating on low carbon steel fabricated from aluminate electrolyte. Vacuum. 2017;144:207-16.
2. Yu J, Zhang Y, Jin X, Chen L, Du J, Xue W. Fabrication and optical emission spectroscopy of enhanced corrosion-resistant CPEO films on Q235 low carbon steel. Surf Coat Tech. 2019;363:411-8.
3. Ma C, Liu J, Zhu X, Xue W, Yan Z, Cheng D, et al. Anticorrosive non-crystalline coating prepared by plasma electrolytic oxidation for ship low carbon steel pipes. Sci Rep. 2020;10(1):15675.
4. Rangel RCC, Cruz NC, Milella A, Fracassi F, Rangel EC. Barrier and mechanical properties of carbon steel coated with SiOx/SiOxCyHz gradual films prepared by PECVD. Surf Coat Tech. 2019;378:124996.
5. Regone NN, Souza MEP, Freire CMA, Ballester M, Rangel EC, Cruz NC. Electrochemical characterization of samples of commercial steel treated with acetylene plasma. Indian J Eng Mater Sci. 2020;27:104-11.
6. Bahadori A. Corrosion and materials selection: a guide for the chemical and petroleum industries. New York: John Wiley & Sons; 2014.
7. Petit-Etienne C, Tatoulian M, Mabille I, Sutter E, Arefi-Khonsari F. Deposition of SiOx-like thin films from a mixture of HMDSO and oxygen by low pressure and DBD discharges to improve the corrosion behaviour of steel. Plasma Process Polym. 2007;4(S1):S562-7.
8. Talbot D, Talbot J. Corrosion science and technology. Boca Raton: CRC Press; 1998.
9. Gentil V. Corrosão. Rio de Janeiro: LTC; 1996.
10. Davis J. Corrosion: understanding the basics. Ohio: ASM International; 2000.
11. Groysman A. Corrosion of a aboveground storage tanks for petroleum distillates and choice of coating systems for their protection of corrosion. In: Harston JD, Ropital F, editors. Corrosion in refineries. Boca Raton: Woodhead; 2007. p. 79-85.
12. Fahmy A, Sabbagh ME, Bedair M, Gangan A, El-Sabbah M, El-Bahy SM, et al. One-step plasma deposited thin SiO x C y films for corrosion resistance of low carbon steel. J Adhes Sci Technol. 2020;0:1-19.
13. Fenili CP, de Souza FS, Marin G, Probst SMH, Binder C, Klein AN. Corrosion resistance of low-carbon steel modified by plasma nitriding and diamond-like carbon. Diamond Relat Mater. 2017;80:153-61.
14. Yang W, Li Q, Liu C, Liang J, Peng Z, Liu B. A comparative study of characterisation of plasma electrolytic oxidation coatings on carbon steel prepared from aluminate and silicate electrolytes. Surf Eng. 2018;34(1):54-62.
15. Yang W, Peng Z, Liu B, Liu W, Liang J. Influence of silicate concentration in electrolyte on the growth and performance of plasma electrolytic oxidation coatings prepared on low carbon steel. J Mater Eng Perform. 2018;27(5):2345-53.
16. Kusmanov SA, Tambovskiy IV, Korableva SS, Dyakov IG, Burov SV, Belkin PN. Enhancement of wear and corrosion resistance in medium carbon steel by plasma electrolytic nitriding and polishing. J Mater Eng Perform. 2019;28(9):5425-32.
17. Wang B, Xue W, Jin X, Zhang Y, Wu Z, Li Y. Combined treatment plasma electrolytic carburizing and borocarburizing on Q235 low-carbon steel. Mater Chem Phys. 2019;221:232-8.
18. Garcia RP, Canobre SC, Costa HL. Microabrasion-corrosion resistance of Ni–Cr superalloys deposited by plasma transferred arc (PTA) welding. Tribol Int. 2020;143:106080.
19. Chu Z, Deng W, Zheng X, Zhou Y, Zhang C, Xu J, et al. Corrosion mechanism of plasma-sprayed fe-based amorphous coatings with high corrosion resistance. J Therm Spray Technol. 2020;29(5):1111-8.
20. Palani V, Kumar A, Vijaya kumar KR, Kumaran P. Vijaya kumar KR, Kumaran P. Investigations on the performance characteristics of carbon nano-tubes, alumina and titanium dioxide based plasma sprayed coatings on AISI 1020 steel. Int J Precis Eng Manuf. 2021;22(2):365-72.
21. Zhang XL, Jiang CP, Zhang FY, Xing YZ. The evaluation of microstructure characteristic and corrosion performance of laser-re-melted fe-based amorphous coating deposited via plasma spraying. Mater Express. 2019;9(9):1100-5.
22. Ma Y, Bai H, Yang B, Yu Q, Zhang Q. Surface modification of carbon steel with plasma chemical vapor deposition for enhancing corrosion resistance in CO_2/brine. IEEE Trans Plasma Sci. 2019;47(5):2652-9.
23. Azioune A, Marcozzi M, Revello V, Pireaux J-J. Deposition of polysiloxane-like nanofilms onto an aluminium alloy by plasma polymerized hexamethyldisiloxane: characterization by XPS and contact angle measurements. Surf Interface Anal. 2007;39(7):615-23.
24. Delimi A, Coffinier Y, Talhi B, Boukherroub R, Szunerits S. Investigation of the corrosion protection of SiOx-like oxide films deposited by plasma-enhanced chemical vapor deposition onto carbon steel. Electrochim Acta. 2010;55(28):8921-7.
25. Vautrin-Ul C, Roux F, Boisse-Laporte C, Pastol JL, Chausse A. Hexamethyldisiloxane (HMDSO)-plasma-polymerised

coatings as primer for iron corrosion protection: influence of RF bias. J Mater Chem. 2002;12(8):2318-24.
26. Fracassi F, d'Agostino R, Palumbo F, Angelini E, Grassini S, Rosalbino F. Application of plasma deposited organosilicon thin films for the corrosion protection of metals. Surf Coat Tech. 2003;174–175:107-11.
27. Ozkaya B, Mitschker F, Ozcan O, Awakowicz P, Grundmeier G. Inhibition of interfacial oxidative degradation during SiO_x plasma polymer barrier film deposition on model organic substrates. Plasma Process Polym. 2015;12(4):392-7.
28. Alexander MR, Short RD, Jones FR, Michaeli W, Blomfield CJ. A study of HMDSO/O2 plasma deposits using a high-sensitivity and -energy resolution XPS instrument: curve fitting of the Si 2p core level. Appl Surf Sci. 1999;137(1-4):179-83.
29. Rangel RCC, Pompeu TC, Barros JL Jr, Antonio CA, Santos NM, Pelici BO, et al. Improvement of the corrosion resistance of carbon steel by plasma deposited thin films. In: Razavi RS, editor. Recent researches in corrosion evaluation and protection. Rijeka: InTech; 2012. p. 91-116.
30. Esbayou M, Bentiss F, Casetta M, Nyassi A, Jama C. Optimization of cold plasma process parameters for organosilicon films deposition on carbon steel: study of the surface pretreatment effect on corrosion protection performance in 3 wt% NaCl medium. J Alloys Compd. 2018;758:148-61.
31. Gangan A, ElSabbagh M, Bedair M, El-Sabbah M, Fahmy A. Plasma power impact on electrochemical performance of low carbon steel coated by plasma thin teos films. Al-Azhar Bull Sci. 2020;31(1):51-8.
32. Benissad N, Boisse-Laporte C, Vallée C, Granier A, Goullet A. Silicon dioxide deposition in a microwave plasma reactor. Surf Coat Tech. 1999;116–119:868-73
33. Ricci M, Dorier JL, Hollenstein C, Fayet P. Influence of argon and nitrogen admixture in HMDSO/O2 plasmas onto powder formation. Plasma Process Polym. 2011;8:108-17.
34. Tsai CH, Li YS, Cheng IC, Chen JZ. O_2/HMDSO-plasma-deposited organic-inorganic hybrid film for gate dielectric of MgZnO thin-film transistor. Plasma Process Polym. 2014;11(1):89-95.
35. Wavhal DS, Zhang J, Steen ML, Fisher ER. Investigation of gas phase species and deposition of SiO_2 films from HMDSO/O2 plasmas. Plasma Process Polym. 2006;3(3):276-87.
36. Blanchard NE, Hanselmann B, Drosten J, Heuberger M, Hegemann D. Densification and hydration of HMDSO plasma polymers. Plasma Process Polym. 2015;12(1):32-41.
37. Lackner JM, Wiesinger M, Kaindl R, Waldhauser W, Heim D, Hartmann P. Plasma polymerization inside tubes in hexamethyldisiloxanes and ethyne glow discharges: effects of deposition atmosphere on wetting and ageing in solvents. Plasma Chem Plasma Process. 2014;34(2):259-69.
38. Gandhiraman RP, Daniels S, Cameron DC. A comparative study of characteristics of SiOx CyHz, TiOx and SiO-TiO oxide-based biocompatible coatings. Plasma Process Polym. 2007;4(S1):S369-73.
39. Khelifa F, Ershov S, Druart M-E, Habibi Y, Chicot D, Olivier M-G, et al. A multilayer coating with optimized properties for corrosion protection of Al. J Mater Chem A Mater Energy Sustain. 2015;3(31):15977-85.
40. Santos NM, Gonçalves TM, Amorim J, Freire CMA, Bortoleto JRR, Durrant SF, et al. Effect of the plasma excitation power on the properties of SiOxCyHz films deposited on AISI 304 steel. Surf Coat Tech. 2017;311:127.
41. Rangel RCC, Cruz NC, Rangel EC. Role of the plasma activation degree on densification of organosilicon films. Materials. 2019;13(1):25.
42. Mancini SD, Nogueira AR, Rangel EC, Cruz NC. Solid-state hydrolysis of postconsumer polyethylene terephthalate after plasma treatment. J Appl Polym Sci. 2013;127(3):1989-96.
43. Vendemiatti C, Hosokawa RS, Rangel RCC, Bortoleto JRR, Cruz NC, Rangel EC. Wettability and surface microstructure of polyamide 6 coated with SiOxCyHz films. Surf Coat Tech. 2015;275:32-40.
44. Oliveira L. Efeitos de tratamentos a plasma na limpeza e na reatividade de aços carbono [dissertation]. Bauru: São Paulo State University; 2008.
45. Granier A, Borvon G, Bousquet A, Goullet A, Leteinturier C, van der Lee A. Mechanisms involved in the conversion of ppHMDSO films into SiO_2-like by oxygen plasma treatment. Plasma Process Polym. 2006;3(4-5):365-73.
46. Hernandez RJ, Giacin JR, Grulke EA. The sorption of water vapor by an amorphous polyamide. J Membr Sci. 1992;65(1-2):187-99.
47. Lee KH, Kim KW, Pesapane A, Kim HY, Rabolt JF. Polarized FT-IR study of macroscopically oriented electrospun nylon-6 nanofibers. Macromolecules. 2008;41(4):1494-8.
48. Porubská M, Szollos O, Konova A, Janigova I, Jaskova M, Jomova K, et al. FTIR spectroscopy study of polyamide-6 irradiated by electron and proton beams. Polym Degrad Stabil. 2012;97(4):523-31.
49. Upadhyay DJ, Cui N-Y, Anderson CA, Brown NMD. Anderson C a., Brown NMD. A comparative study of the surface activation of polyamides using an air dielectric barrier discharge. Colloids Surf A Physicochem Eng Asp. 2004;248(1-3):47-56.
50. Hooper AE, Tompkins HG. Convenient calibration of FTIR peak 'size' for thin organic/polymer films. Surf Interface Anal. 2001;31(9):805-8.
51. Rau C, Kulisch W. Mechanisms of plasma polymerization of various silico-organic monomers. Thin Solid Films. 1994;249(1):28-37.
52. Lommatzsch U, Ihde J. Plasma polymerization of HMDSO with an atmospheric pressure plasma jet for corrosion protection of aluminum and low-adhesion surfaces. Plasma Process Polym. 2009;6(10):642-8.
53. Gengenbach TR, Griesser HJ. Post-deposition ageing reactions differ markedly between plasma polymers deposited from siloxane and silazane monomers. Polymer. 1999;40(18):5079-94.
54. Benítez F, Martínez E, Esteve J. Improvement of hardness in plasma polymerized hexamethyldisiloxane coatings by silica-like surface modification. Thin Solid Films. 2000;377-378:109-14.
55. Grundmeier G, Thiemann P, Carpentier J, Shirtcliffe N, Stratmann M. Tailoring of the morphology and chemical composition of thin organosilane microwave plasma polymer layers on metal substrates. Thin Solid Films. 2004;446(1):61-71.
56. Grundmeier G, Stratmann M. Interfacial processes during plasma polymer deposition on oxide covered iron. Thin Solid Films. 1999;352(1-2):119-27.
57. Kondoh E, Asano T, Nakashima A, Komatu M. Effect of oxygen plasma exposure of porous spin-on-glass films. J Vac Sci Technol B. 2000;18(3):1276. http://dx.doi.org/10.1116/1.591374.
58. Schäfer J, Horn S, Foest R, Brandenburg R, Vašina P, Weltmann K-D. Complex analysis of SiOxCyHz films deposited by an atmospheric pressure dielectric barrier discharge. Surf Coat Tech. 2011;205:S330-4.
59. Lasorsa C, Morando PJ, Rodrigo A. Effects of the plasma oxygen concentration on the formation of SiOxCy films by low temperature PECVD. Surf Coat Tech. 2005;194(1):42-7.
60. Wang YH, Kumar R, Zhou X, Pan JS, Chai JW. Effect of oxygen plasma treatment on low dielectric constant carbon-doped silicon oxide thin films. Thin Solid Films. 2005;473(1):132-6.
61. Coclite AM, Milella A, d'Agostino R, Palumbo F. On the relationship between the structure and the barrier performance of plasma deposited silicon dioxide-like films. Surf Coat Tech. 2010;204(24):4012-7.
62. Ghali N, Vivien C, Mutel B, Rives A. Multilayer coating by plasma polymerization of TMDSO deposited on carbon steel: synthesis and characterization. Surf Coat Tech. 2014;259:504-16.

63. Chung C, Lee M, Choe EK. Characterization of cotton fabric scouring by FT-IR ATR spectroscopy. Carbohydr Polym. 2004;58(4):417-20.
64. Schuttlefield JD, Grassian VH. ATR–FTIR Spectroscopy in the Undergraduate Chemistry Laboratory. Part I: fundamentals and Examples. J Chem Educ. 2008;85(2):279.
65. Technologies P. Product Data Sheet: MIRacle ATR-Fast and Easy IR Sampling. Pike Technol. 2015. https://www.piketech.com/files/pdfs/MIRaclePDS1213.pdf (accessed 8 Aug 2016).
66. Boscher ND, Choquet P, Duday D, Verdier S. Chemical compositions of organosilicon thin films deposited on aluminium foil by atmospheric pressure dielectric barrier discharge and their electrochemical behaviour. Surf Coat Tech. 2010;205(7):2438-48.
67. Lehmann A, Rupf S, Schubert A, Zylla I-M, Seifert HJ, Schindler A, et al. Plasma deposited silicon oxide films for controlled permeation of copper as antimicrobial agent. Clin Plasma Med. 2015;3(1):3-9.
68. Grill A, Neumayer DA. Structure of low dielectric constant to extreme low dielectric constant SiCOH films: fourier transform infrared spectroscopy characterization. J Appl Phys. 2003;94(10):6697-707.
69. Inomata K, Ha H, Chaudhary KA, Koinuma H. Open air deposition of SiO_2 film from a cold plasma torch of tetramethoxysilane-H2-Ar system. Appl Phys Lett. 1994;64(1):46-8.
70. Kurosawa S, Choi BG, Park JW, Aizawa H, Shim KB, Yamamoto K. Synthesis and characterization of plasma-polymerized hexamethyldisiloxane films. Thin Solid Films. 2006;506-507:176-9.
71. Vautrin-Ul C, Boisse-Laporte C, Benissad N, Chausse A, Leprince P, Messina R. Plasma-polymerized coatings using HMDSO precursor for iron protection. Prog Org Coat. 2000;38(1):9-15.
72. Schäfer J, Foest R, Quade A, Ohl A, Weltmann K-D. Local deposition of SiO x plasma polymer films by a miniaturized atmospheric pressure plasma jet (APPJ). J Phys D Appl Phys. 2008;41(19):194010.
73. Zajíčková L, Janca L, Perina V. Characterization of silicon oxide thin films deposited by plasma enhanced chemical vapour deposition from octamethylcyclotetrasiloxane/oxygen feeds. Thin Solid Films. 1999;338(1-2):49-59.
74. Wang H, Yang L, Chen Q. Investigation of microwave surface-wave plasma deposited SiO x coatings on polymeric substrates. Plasma Sci Technol. 2014;16(1):37-40.
75. Huang CH, Wang NF, Tsai YZ, Liu CC, Hung CI, Houng MP. The formation of a SiOx interfacial layer on low-k SiOCH materials fabricated in ULSI application. Mater Chem Phys. 2008;110(2-3):299-302.
76. Supiot P, Vivien C, Granier A, Bousquet A, Mackova A, Escaich D, et al. Growth and modification of organosilicon films in PECVD and remote afterglow reactors. Plasma Process Polym. 2006;3(2):100-9.
77. Lanford WA, Rand MJ. The hydrogen content of plasma-deposited silicon nitride. J Appl Phys. 1978;49(4):2473-7.
78. Milella A, Creatore M, Blauw MA, van de Sanden MCM. Remote plasma deposited silicon sioxide-like film densification by means of RF substrate biasing: film chemistry and morphology. Plasma Process Polym. 2007;4(6):621-8.
79. Nowling GR, Yajima M, Babayan SE, Moravej M, Yang X, Hoffman W, et al. Chamberless plasma deposition of glass coatings on plastic. Plasma Sources Sci Technol. 2005;14(3):477-84.
80. Grill A, Patel V, Rodbell KP, Huang E, Baklanov MR, Mogilnikov KP, et al. Porosity in plasma enhanced chemical vapor deposited SiCoH dielectrics: a comparative study. J Appl Phys. 2003;94(5):3427-35.
81. Wavhal DS, Zhang J, Steen ML, Fisher ER. Investigation of gas phase species and deposition of SiO_2 films from HMDSO/O2 plasmas. Plasma Process Polym. 2006;3(3):276-87.
82. Choudhury AJ, Barve SA, Chutia J, Kakati H, Pal AR, Jagannath, et al. Effect of impinging ion energy on the substrates during deposition of SiOx films by radiofrequency plasma enhanced chemical vapor deposition process. Thin Solid Films. 2011;519(22):7864-70.
83. Clergereaux R, Calafat M, Benitez F, Escaich D, Savin de Larclause I, Raynaud P, et al. Comparison between continuous and microwave oxygen plasma post-treatment on organosilicon plasma deposited layers: effects on structure and properties. Thin Solid Films. 2007;515(7-8):3452-60.
84. Cong C, Cui C, Meng X, Zhou Q. Stability of POSS crosslinks and aggregates in tetrafluoroethylene- propylene elastomers/OVPOSS composites exposed to hydrochloric acid solution. Polym Degrad Stabil. 2014;100:29-36.
85. Kron J, Amberg-schwab S, Schottner G. Functional coatings on glass using ORMOCER®-systems. J Sol-Gel Sci Technol. 1994;2(1-3):189-92.
86. Xie XN, Chung HJ, Sow CH, Wee ATS. Oxide growth and its dielectrical properties on alkylsilated native-SiO_2/Si surface. Chem Phys Lett. 2004;388(4-6):446-51.
87. Massines F, Gherardi N, Fornelli A, Martin S. Atmospheric pressure plasma deposition of thin films by Townsend dielectric barrier discharge. Surf Coat Tech. 2005;200(5-6):1855-61.
88. Theil J, Brace JG, Knoll RW. Carbon content of silicon oxide films deposited by room temperature plasma enhanced chemical vapor deposition of hexamethyldisiloxane and oxygen. J Vac Sci Technol A. 1994;12(4):1365-70.
89. Fu CJ, Zhan ZW, Yu M, Li SM, Liu JH, Dong L. Influence of Zr / Si molar ratio on structure, morphology and corrosion resistance of organosilane coatings doped with zirconium (IV) n-propoxide. Int J Electrochem Sci. 2014;9:2603-19.
90. Kudriavtsev Y, Asomoza-Palacio R, Manzanilla-Naim L. New insight into water-obsidian interaction. Rev Mex Fis. 2017;63:19-25.
91. Blanchard NE, Naik VV, Geue T, Kahle O, Hegemann D, Heuberger M. Response of plasma-polymerized hexamethyldisiloxane films to aqueous environments. Langmuir. 2015;31(47):12944-53.
92. van Hest MFAM, Klaver A, Schram DC, van de Sanden MCM. Argon-oxygen plasma treatment of deposited organosilicon thin films. Thin Solid Films. 2004;449(1-2):40-51.
93. Soller BR, Shuman RF, Ross RR. Application of emission spectroscopy for profile control during oxygen RIE of thick photoresist. J Electrochem Soc. 1984;131(6):1353-6.
94. Steinbrüchel C, Curtis BJ, Lehmann HW, Widmer R. Diagnostics of low-pressure oxygen RF plasmas and the mechanism for polymer etching: a comparison of reactive sputter etching and magnetron sputter etching. IEEE Trans Plasma Sci. 1986;14(2):137-44.
95. Creatore M, Palumbo F, d'Agostino R. Deposition of SiO x films from hexamethyldisiloxane/oxygen radiofrequency glow discharges : process optimization by plasma diagnostics. Plasma Polym. 2002;7(3):291-310.
96. Bruce RL, Lin T, Phaneuf RJ, Oehrlein GS, Bell W, Long B, et al. Molecular structure effects on dry etching behavior of Si-containing resists in oxygen plasma. J Vac Sci Technol B. 2010;28(4):751-7.
97. Magni D, Deschenaux C, Hollenstein C, Creatore A, Fayet P. Oxygen diluted hexamethyldisiloxane plasmas investigated by means of in situ infrared absorption spectroscopy and mass spectrometry. J Phys D Appl Phys. 2001;34(1):87-94.
98. Albuquerque MDF, Santos E Jr, Perdone RRT, Simao RA. Effect of self-bias voltage on the wettability, chemical functionality and nanomechanical properties of hexamethyldisiloxane films. Thin Solid Films. 2014;564:73-8.
99. Sun M, Yerokhin A, Matthews A, Thomas M, Laukart A, von Hausen M, et al. characterisation and electrochemical evaluation of plasma electrolytic oxidation coatings on magnesium with

plasma enhanced chemical vapour deposition post-treatments. Plasma Process Polym. 2016;13(2):266-78.
100. Han L, Mandlik P, Gartside J, Wagner S, Silvernail JA, Ma R-Q, et al. Properties of a permeation barrier material deposited from hexamethyl disiloxane and oxygen. J Electrochem Soc. 2009;156(2):H106-14.
101. Coclite AM, Milella A, Palumbo F, Fracassi F, d'Agostino RA. Chemical study of plasma-deposited organosilicon thin films as low-*k* dielectrics. Plasma Process Polym. 2009;6(8):512-20.
102. Tait WS. An introduction to electrochemical corrosion testing for practicing engineers and scientists. Racine: Pair O Docs Publications; 1994.
103. Yu D, Tian J, Dai J, Wang X. Corrosion resistance of three-layer superhydrophobic composite coating on carbon steel in seawater. Electrochim Acta. 2013;97:409-19.
104. Barranco V, Carpentier J, Grundmeier G. Correlation of morphology and barrier properties of thin microwave plasma polymer films on metal substrate. Electrochim Acta. 2004;49(12):1999-2013.